



Universidade do Estado do Rio de Janeiro  
Centro de Tecnologia e Ciências  
Instituto de Química

Ana Cristina Corrêa de Araujo

**Theoretical Study of the electrostatic behavior of *Saccharomyces cerevisiae*  
yeast cell using Poisson-Boltzmann equation**

Rio de Janeiro

2020

CATALOGAÇÃO NA FONTE  
UERJ / REDE SIRIUS / BIBLIOTECA CTC/Q

A663 Araujo, Ana Cristina Corrêa de.

Theoretical Study of the electrostatic behavior of *Saccharomyces cerevisiae* yeast cell using Poisson-Boltzmann equation. – 2020.

68 f.

Orientador: Eduardo Rocha de Almeida Lima

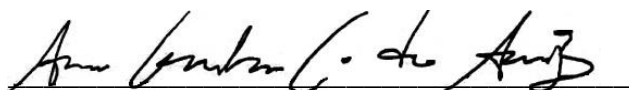
Coorientador: Nathalia Salles Vernin Barbosa

Dissertação (Mestrado) – Universidade do Estado do Rio de Janeiro.  
Instituto de Química.

1. Leveduras (Fungos) – Teses. 2. *Saccharomyces cerevisiae* – Teses. 3. Equação de Poisson-Boltzmann – Teses. I. Lima, Eduardo Rocha de Almeida. II. Barbosa, Nathalia Salles Vernin. III. Universidade do Estado do Rio de Janeiro. Instituto de Química. IV. Título.

CDU 577.3

Autorizo, apenas para fins acadêmicos e científicos, a reprodução total ou parcial desta dissertação, desde que citada a fonte.



Assinatura

20/08/2021

Data

Ana Cristina Corrêa de Araujo

**Theoretical Study of the electrostatic behavior of *Saccharomyces cerevisiae* yeast cell  
using Poisson-Boltzmann equation**



Dissertação apresentada, como requisito parcial para obtenção de título de Mestre em Engenharia Química, ao Programa de Pós-graduação em Engenharia Química, da Universidade do Estado do Rio de Janeiro. Área de concentração: Processos Químicos, Petróleo e Meio Ambiente.

Orientadores: Prof. Dr. Eduardo Rocha de Almeida Lima

Prof<sup>a</sup>. Dr<sup>a</sup>. Nathalia Salles Vernin Barbosa

Rio de Janeiro

2020

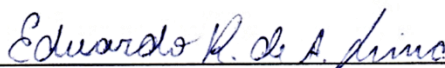
Ana Cristina Corrêa de Araujo

**Theoretical Study of the electrostatic behavior of *Saccharomyces cerevisiae* yeast cell using Poisson-Boltzmann equation**

Dissertação apresentada, como requisito parcial para obtenção de título de Mestre em Engenharia Química, ao Programa de Pós-graduação em Engenharia Química, da Universidade do Estado do Rio de Janeiro. Área de concentração: Processos Químicos, Petróleo e Meio Ambiente.

Aprovada em 17 de fevereiro de 2020.

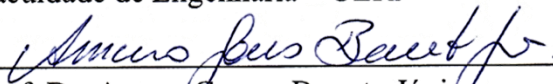
Banca Examinadora:



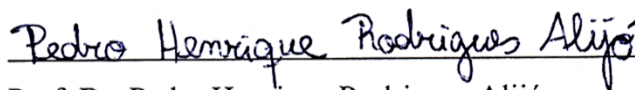
Prof. Dr. Eduardo Rocha de Almeida Lima (Orientador)  
Instituto de Química – UERJ



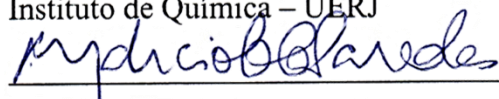
Prof.<sup>a</sup>. Dr.<sup>a</sup>. Nathalia Salles Vernin Barbosa (Orientadora)  
Faculdade de Engenharia – UERJ



Prof. Dr. Amaro Gomes Barreto Júnior  
Universidade Federal do Rio de Janeiro



Prof. Dr. Pedro Henrique Rodrigues Alijó  
Instituto de Química – UERJ



Prof. Dr. Márcio Luis Lyra Paredes  
Instituto de Química – UERJ



Prof. Dr. Fernando Luis Barroso da Silva  
Universidade de São Paulo

Rio de Janeiro

2020

## **AGRADECIMENTOS**

Aos meus pais, Eduardo e Denilda, que me apoiaram muito nesta etapa da minha vida.

Aos meus orientadores, Eduardo e Nathalia, pela disponibilidade, paciência e orientação.

Aos demais professores do PPGEQ/UERJ pelos diversos ensinamentos.

Aos amigos e colegas do PPGEQ/UERJ pela amizade, em especial à Thais e ao Everson que foram os que mais me apoiaram ao longo desses 2 anos.

À CAPES pelo apoio financeiro concedido.

## RESUMO

ARAUJO, Ana Cristina Corrêa. *Estudo teórico do comportamento eletrostático da levedura Saccharomyces cerevisiae usando a equação de Poisson-Boltzmann*. 2020. 68 f. Dissertação (Mestrado em Engenharia Química) – Instituto de Química, Universidade do Estado do Rio de Janeiro, 2020.

A investigação do comportamento eletrostático e das propriedades de superfície de células e sistemas biológicos é de grande importância para o entendimento de processos biotecnológicos como captação de metais pesados de solução, formação de biofilmes, processos de biocorrosão, entre outros. Leveduras estão presentes na natureza e em inúmeros processos científicos e industriais onde as forças eletrostáticas são predominantes, como processos de adesão, flotação e coagulação. A superfície da parede celular das leveduras contém grupos funcionais ácidos e básicos – e.g. carboxila, fosforila, hidroxila, e amino – que sob diferentes condições podem estar ionizados. A protonação e desprotonação desses grupos influencia a carga na superfície da célula e promove uma distribuição entre o meio e a superfície da célula, criando uma superfície regulada pela carga. Nesse trabalho, o potencial eletrostático da levedura *Saccharomyces cerevisiae* foi estudado e a partir dele um valor para o potencial zeta foi estimado. Os cálculos foram feitos usando dois modelos baseados na equação de Poisson-Boltzmann, um modelo de regulação de cargas e um modelo de densidade de carga volumétrica. Os dois modelos diferem em como eles descrevem a carga na superfície da célula de levedura, o primeiro considera a carga variando na área superficial da célula e o segundo modelo considera a carga variando dentro de um volume na parede celular. Os potenciais zeta estimados pelos dois modelos foram comparados a resultados experimentais para checar a acurácia dos modelos. Cálculos foram feitos para soluções aquosas com duas forças iônicas diferentes, 1 mM e 10 mM. Resultados mostram que os dois modelos conseguem descrever bem os pontos experimentais de potencial zeta para diferentes valores de pH, com o modelo de densidade de carga volumétrica se aproximando um pouco mais dos pontos que o modelo de regulação de carga na superfície. Em geral, os resultados para a força iônica de 10 mM dos dois modelos conseguem descrever melhor o formato dos pontos. Alguns parâmetros dos modelos relacionados a caracterização da superfície da parede celular da levedura (grupos funcionais) foram estimados usando o método de mínimos quadrados, e os resultados dos modelos usando os parâmetros estimados mostraram grande melhoria na maioria dos casos. Além disso, estes mesmos parâmetros foram analisados usando uma simulação de Monte Carlo e uma decomposição QR da matriz de sensibilidade do modelo de regulação de cargas para melhor entendimento da relação entre os parâmetros e o modelo. Nas análises foram encontrados aonde estão localizados os valores de parâmetros que melhor representam os pontos experimentais e também a quais parâmetros o modelo parece ser mais ou menos sensível.

Palavras-chave: Levedura. Potencial zeta. Regulação de carga. Equação de Poisson-Boltzmann.

## ABSTRACT

ARAUJO, Ana Cristina Corrêa. *Theoretical Study of the electrostatic behavior of Saccharomyces cerevisiae yeast cell using Poisson-Boltzmann equation*. 2020. 68 f. Dissertação (Mestrado em Engenharia Química) – Instituto de Química, Universidade do Estado do Rio de Janeiro, 2020.

The investigation of the electrostatic behavior and surface properties of cell surfaces in biological systems is of great importance for understanding biological process as metal uptake from solution, biofilm formations, biocorrosion processes, among others. Yeast cells are present in nature and in a number of scientific and industrial processes where electrostatic forces are predominant, such as adhesion processes, flotation and aggregation. The cell wall surface of yeast cells is composed of proteins and glycoproteins that contain many acid-base functional groups – e.g. carboxyl, phosphoryl, hydroxyl, and amine – that under different conditions can be ionized. The protonation or deprotonation of these groups influences the surface charge and promotes a charge distribution between the medium and the cell surface, creating a charge regulated surface. In this work, the electrostatic potential of the *Saccharomyces cerevisiae* yeast cell was studied and a value for the zeta potential was estimated. Calculations were performed using two models based on the Poisson-Boltzmann equation, the charge regulation on the surface model and the charge regulated volumetric density charge model. The two models differ in the way they describe the charge on the yeast cell surface, while the first considers a charge on the cell wall surface area the second model considers the charge varying over the volume of the cell wall. The zeta potential calculated using both models were then compared to experimental results to check for the accuracy of the models. Calculations were performed for aqueous solutions with two different ionic strengths, 1 mM and 10 mM. Results show that both models are able to describe experimental zeta potential points for different pH values, with the volumetric charge density model showing a slightly better fit than the charge regulation on the surface model. In general, the results for ionic strength of 10 mM for both models could describe better the shape of experimental points than the results for 1 mM. Some important parameters of the model related to the characterization of the yeast cell wall (functional groups) were estimated using the least-squares method, and results of the model with the estimated parameters showed great improvement in most cases. The same parameters were then further analyzed using a Monte Carlo simulation and a QR decomposition of the sensitive matrix of the charge regulation model to check the relation between the parameters and the model. In the analysis it was found a range for which the parameters can best describe experimental points and it was also possible to identify which parameters the model are most and least sensitive to.

Keywords: Yeast cell. Zeta potential. Charge regulation. Poisson-Boltzmann equation.

## LISTA DE FIGURAS

Figure 1 – The yeast cell wall.....	13
Figure 2 - Components of the electrical double layer .....	20
Figure 3 – Expected curve of the electrostatic potential for the charge regulation model .....	26
Figure 4 – Algorithm for the charge regulation model.....	27
Figure 5 – Expected electrostatic potential for the volumetric charge density model .....	28
Figure 6 – Algorithm for the volumetric charge density model .....	30
Figure 7 – Electrostatic potential of the <i>S. cerevisiae</i> yeast cell wall calculated by the charge regulation on the surface model at pH=7.0. ....	34
Figure 8 – Electrostatic potential of <i>S. cerevisiae</i> yeast cell calculated by the charge regulation on the surface model using the effective number of groups at pH=7.0 ....	37
Figure 9 – Modeled zeta potential of <i>S. cerevisiae</i> as a function of pH for 10 mM with effectiveness coefficient equal to $3.05 \times 10^{-4}$ .....	38
Figure 10 – Modeled zeta potential of <i>S. cerevisiae</i> as a function of pH for 1 mM with effectiveness coefficient equal to $1.57 \times 10^{-4}$ .....	39
Figure 11 – Modeled zeta potential for 10 mM with estimation of effectiveness coefficient and $pK_a$ .....	40
Figure 12 – Modeled zeta potential for 1 mM with estimation of the effectiveness coefficient and $pK_a$ .....	41
Figure 13 – Zeta potential of <i>S. cerevisiae</i> as a function of pH for 10 mM with estimation of effectiveness coefficient and $pK_a$ using a wider range.....	44
Figure 14 – Zeta potential of <i>S. cerevisiae</i> as a function of pH for 1 mM with estimation of effectiveness coefficient and $pK_a$ using a wider range.....	45
Figure 15 – Electrostatic potential profile computed by the charge-regulated volume charge density model for ionic strength of 10 mM (NaCl).....	47
Figure 16 – Electrostatic potential profile computed by the charge-regulated volume charge density model for ionic strength of 1 mM (NaCl).....	48
Figure 17 – Electrostatic potential profile computed by the charge-regulated volume charge density model with the effectiveness coefficient for ionic strength of 10 mM (NaCl).....	51
Figure 18 – Electrostatic potential of <i>S. cerevisiae</i> as a function of pH for ionic strength of 10 mM for the two models studied in this work.....	52

Figure 19 – Electrostatic potential profile computed by the charge-regulated volume charge density model with the effectiveness coefficient for ionic strength of 10 mM (NaCl).	53
Figure 20 – Electrostatic potential of <i>S. cerevisiae</i> as a function of pH for ionic strength of 1mM for the two models studied in this work.....	54
Figure 21 – pK <sub>a</sub> parameters of Monte Carlo simulation.....	56
Figure 22 – Estimated effectiveness coefficient for the pK <sub>a</sub> parameters.....	57
Figure 23 – Elementary volume .....	65

## LISTA DE TABELAS

Table 1 – Fixed parameters of charge regulation model .....	31
Table 2 – Potentiometric titration data of <i>S. cerevisiae</i> .....	32
Table 3 – Functional groups parameters .....	35
Table 4 – Estimated functional groups parameters (effectiveness coefficient and pK <sub>a</sub> ) .....	40
Table 5 – Wider pK <sub>a</sub> range found in literature of the functional groups .....	42
Table 6 – Results for optimization with broader pK <sub>a</sub> ranges .....	43
Table 7 – Number of groups parameters for the charge-regulated volume charge density model .....	46
Table 8 – Estimation results for the volumetric charge density model .....	49
Table 9 – Normalized sensitivity matrix of the charge regulation on the surface model .....	58
Table 10 – Results of the QR decomposition of the sensitivity matrix .....	58
Table 11 – Linearized font terms for the dimensionless PB equations .....	67

## SUMÁRIO

<b>INTRODUCTION</b> .....	10
<b>1 LITERATURE REVIEW</b> .....	13
1.1 <i>Saccharomyces cerevisiae</i> cell wall .....	13
1.2 <b>Poisson-Boltzmann equation</b> .....	16
1.3 <b>Poisson-Boltzmann equation with fixed charges</b> .....	17
1.4 <b>Zeta potential</b> .....	18
1.5 <b>Parameter estimation</b> .....	20
1.6 <b>Parameter analysis methods</b> .....	21
1.6.1 <u>Monte Carlo method</u> .....	21
1.6.2 <u>Sensitive parameter analysis</u> .....	22
<b>2 MODEL AND METHODS</b> .....	24
2.1 <b>Yeast surface charge regulation function</b> .....	24
2.2 <b>Charge regulation on the surface model</b> .....	25
2.3 <b>Charge-regulated volume charge density model</b> .....	28
2.4 <b>Parameters of the model</b> .....	31
<b>3 RESULTS AND DISCUSSION</b> .....	34
3.1 <b>Charge regulation on the surface</b> .....	34
3.2 <b>Constant volume charge density model</b> .....	46
3.3 <b>Parametric analysis results</b> .....	54
3.3.1 <u>Monte Carlo simulation</u> .....	55
3.3.2 <u>Sensitivity matrix analysis</u> .....	57
<b>CONCLUSION</b> .....	60
<b>REFERENCES</b> .....	62
<b>APPENDIX A – Finite Volume Method</b> .....	65

## INTRODUCTION

The DLVO (Derjaguin-Landau-Verwey-Overbeek) theory, although not originally designed to explain the behavior of biological colloids, has been extensively used in biological studies. It has been used to explain many bioprocesses in which surface interactions play a key role such as adhesion of microbials to surfaces, formation of biofilm, aggregation and flocculation, heavy metal biosorption, among others (ARAÚJO et al., 2009; RAO; SUBRAMANIAN, 2007; ASRI et al., 2017; ROGOWSKA et al., 2018).

In biological colloids, the DLVO theory has been used in both qualitative and quantitative models for predicting surface properties, forces and free energy. While qualitative results have shown some success, quantitative models have often failed to describe microbiological systems adequately (HERMANSSON, 1999). Biological cell surfaces usually are more complex and heterogeneous than the surface of non-biological colloidal particles and this can have an impact on the results predicted by the classical DLVO theory. For instance, interactions involving macromolecules attached to the cell surface can influence both surface charge distribution and steric interactions (RIJNAARTS et al., 1999). To account for other types of effects an extended DLVO theory was developed considering other types of interactions besides the ones described in the classical theory (van der Waals and double layer interactions) with the most relevant interaction being the Lewis acid-base interactions (SHARP; DICKINSON, 2005). The acid-base interactions are based on electron-donating and electron-accepting energies and, according to van Oss (1989), can be 10-100 times stronger than the van der Waals interaction.

Experimental studies have shown the importance of the electric double layer in microbial adhesion interactions. However, models considering only double layer interactions often fail to reproduce accurately experimental observations (HERMANSSON, 1999). By introducing an acid-base interaction term, some models have shown improvement in describing electrical properties in biological system (POORTINGA et al., 2002). Regarding the zeta potential of biological surfaces, an important measure in indicating the stability of colloids, it is possible to point out two models that have been successful in predicting experimental zeta potential results: (i) a charge regulation model, used by Hong and Brown (2008), was able to portray the experimental zeta potential results of two bacteria, *Escherichia coli* and *Bacillus brevis*, in different ionic strengths; (ii) Barbosa, Lima and Tavares (2015) using a different model, which considers the cell wall with a volumetric charge density, was also able to describe experimental zeta potential points of the *B. brevis* bacteria.

With this knowledge in mind, the goal of this study was to analyze the electrostatic behavior of the *Saccharomyces cerevisiae* yeast cell using the same models as Hong and Brown (2008) and Barbosa, Lima and Tavares (2015). The zeta potential of the *S. cerevisiae* yeast cell was modeled and compared to experimental zeta potential data. The two models used in this study apply the Poisson-Boltzmann equation to describe the double layer interactions; however, the main difference is in the way they describe the acid-base interactions that happen within the macromolecules present on the cell wall. While the first model studied considers the contribution of acid-base interactions only on the surface area of the cell wall, the second model considers this contribution not only on the surface area, but in the volume of the cell wall. When solving both models, parameters of the *S. cerevisiae* cell surface were necessary to complete the acid-base interactions calculations. Data for these parameters were taken from experiments found in the literature and values for the parameters were estimated and analyzed by different methods that will be discussed further on.

*S. cerevisiae* was chosen as the object of the study first to check if the models could accurately describe yeast surfaces as well as they did for bacterial surfaces, given that the cell wall of bacteria and yeast cells shows some similarities. As in bacteria, yeast cell walls also possess ionizable functional groups that under different circumstances can be protonated or deprotonated, creating a charge on the surface that varies with the ionization rate of these groups (DENGIS; ROUXHET, 1997). Another good reason for studying the *S. cerevisiae* cell is the fact that this yeast is widely present in natural surfaces and industrial processes. This way it can be easily incorporated in new technologies, showing an interesting potential in the wastewater treatment area, where some yeast strains have shown a good capacity for the biosorption of heavy metals, for example (NAEEM; WOERTZ; FEIN, 2006; ASRI et al., 2017). And last but not least, another factor that played an important role in the choice of *S. cerevisiae* for this study was the amount of experimental data available for it in the literature. Since experiments were not performed during this work, it was important to find a microorganism with plenty of experimental data available to help obtain parameters and evaluate results calculated by the models. Due to its abundance and relevance, the *S. cerevisiae* yeast cell has been greatly studied and for this reason a numerous amount of experimental data on it is available in the literature.

In summary, the objective of the study is:

- A) Calculate the electrostatic potential profile on the *S. cerevisiae* yeast cell using two different models based on the Poisson-Boltzmann equation: (i) charge regulation on the surface model; (ii) charge-regulated volumetric charge density model.
- B) Estimate zeta potential values for the *S. cerevisiae* from the calculated electrostatic potential profile.
- C) Compare the calculated zeta potential with experimental zeta potential values for the *S. cerevisiae* available in literature.

After this introduction presenting the general idea and objectives of the study, in chapter 1, the literature review, essential parts of the studied system will be described, they are the yeast cell surface and acid-base interactions that configures the cell surface charge, the Poisson-Boltzmann equations used in the models, the definition of the so-called zeta potential and a description of the methods used in the parameter estimation and analysis. In the second chapter, models and methods, the information provided in the literature review chapter are connected to develop the models used in the study in order to calculate the electric potential of *S. cerevisiae*. The third chapter is focused on analyzing the results obtained by the models to describe the electric behavior of *S. cerevisiae*. Also, in this chapter results for parameter estimation are presented and analyzed. To finish, a conclusion is presented to summarize the most relevant observations made during the study.

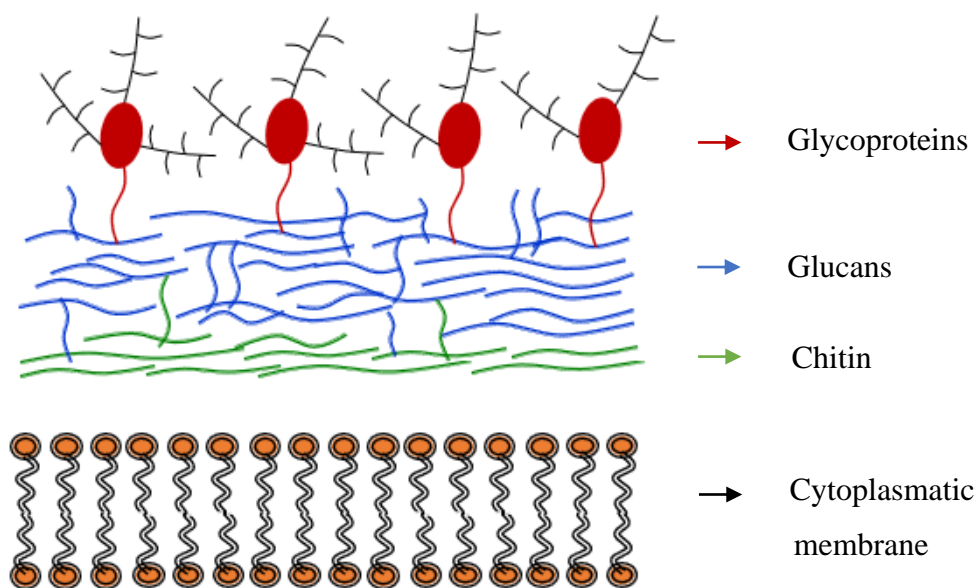
## 1 LITERATURE REVIEW

### 1.1 *Saccharomyces cerevisiae* cell wall

Cell walls are complex and dynamic structures that involve the cytoplasmic membrane and give the cell support and protection from changes in the environment. Moreover, they allow the cells to interact with other components. In order to protect the cell from physical stress, the cell wall must possess enough mechanical strength, and to be able to interact with other components it is fundamental to bind to particles on its surroundings. Many molecules are involved in performing these functions and that is why the cell wall is a complex structure. The yeast cell wall is primarily composed of glycoproteins and polysaccharides such as chitin, glucans and mannans (BOWMAN; FREE, 2006).

In Figure 1 we can see a simplified schematic representation of the *Saccharomyces cerevisiae* yeast cell wall characterized by a thin layer of chitin on the inner part of the cell wall, above it a thicker layer of glucans is found and on the most outer surface of the cell there is a layer of glycoproteins, which are proteins highly modified with polysaccharides chains.

Figure 1 – The yeast cell wall



The chitin component, although representing only about 2% of the cell wall dry weight, is structurally very important as it is responsible for giving the cell wall strength and flexibility. The glucan component is also important for the structure of the cell wall. Besides providing mechanical strength and integrity to the cell wall, this component is responsible for linking the chitin layer to the glycoproteins. The glycoproteins components of the cell wall are located on the most outer surface. They are the ones responsible for the interaction of the cell wall with other particles, their functions vary from mediating adhesion to surfaces and absorption of molecules to transmitting signals and even protecting the cell against foreign substances (BOWMAN; FREE, 2006). Also, it is mainly on the glycoproteins that very important components responsible for surface charge on the cell wall are located – they are called functional groups (DENGIS; ROUXHET, 1997).

Comparing the yeast cell wall to the cell wall of bacteria some differences and some similarities are noticed. For instance, while the yeast cell wall has a chitin and glucan inner layer, bacteria cell walls have a peptidoglycan inner layer, which can be thin as in the Gram-negative or thick as in the Gram-positive bacteria (POORTINGA et al., 2002). At the same time, when it comes to the outer layer of bacteria and yeast cell walls, both seem to be composed by glycoproteins (POORTINGA et al., 2002). So, when talking about the electrostatic behavior of both yeast and bacteria cells, they seem to be related to the same components. With this in mind it seems reasonable that we use the same relations applied in describing the functional groups of bacteria cells to yeast cells.

The functional groups are structures that can be ionized under different conditions and this creates a charge on the cell surface that is dependent on the ionization rate of the groups. The functional group types present on a cell surface may differ from one organism to another, but all of them contribute in a similar way to the cell surface charge: an acidic group ( $>AH$ ) can donate a proton to the medium contributing negatively to the surface charge, and a basic group ( $>B$ ) can accept a proton from the medium contributing positively to the charge (HONG; BROWN, 2008). Relations describing acidic and basic functional group can be seen in equations (1) and (2), respectively.



The main functional groups present on the yeast cell wall are the carboxyl, phosphoryl, hydroxyl and amine groups. The carboxyl and amine groups are mainly linked to the protein part of the glycoproteins while the hydroxyl and phosphoryl are related to the glycans part, mostly to mannan and phosphorylated mannan (ZHANG et al, 2010). Only the amine group on the yeast cell is a basic functional group, the other three groups are acidic, so unless the amount of the amine group is much higher than the other groups, we expect the surface charge on the yeast cell to be mainly negative.

When calculating the surface charge on a yeast or bacteria cell, it is important to determine which groups are in their ionized state and which are not, the groups that are ionized contribute to the cell surface charge and the groups in their neutral state do not. A frequently calculated property for describing a strongly ionized system is the dissociation constant ( $K_a$ ). The dissociation constant of the basic and acidic groups related to the descriptions in equations (1) and (2) are represented on equations (3) and (4).

$$K_{a,acid} = \frac{C_{H_s^+} C_{A^-}}{C_{AH}} \quad (3)$$

$$K_{a,basic} = \frac{C_{H_s^+} C_B}{C_{BH^+}} \quad (4)$$

Where  $C_{A^-}$  and  $C_B$  are the concentrations of acidic and basic groups that are deprotonated,  $C_{AH}$  and  $C_{BH^+}$  are the concentrations of acidic and basic groups that are protonated and  $C_{H_s^+}$  is the local concentration of protons at the surface.

Looking at equations (3) and (4) it is possible to notice that the dissociation constant of the functional groups is a function of the local proton concentration at the surface ( $C_{H_s^+}$ ). This concentration is not the same as the proton concentration in the bulk solution, given that the charge on the cell surface has influence over all ionic concentrations near it.

Estimations for the dissociation constant of the functional groups can be obtained through potentiometric titration experiments, and their values can provide valuable insight into how the functional groups influence the surface charge and consequently other surface properties, as for example, the zeta potential (HONG; BROWN, 2006, 2008).

## 1.2 Poisson-Boltzmann equation

The Poisson equation, that relates the volumetric charge density ( $\rho$ ) with the electrostatic potential ( $\psi$ ) can be written in the form of (LIMA, 2008):

$$\varepsilon_0 \nabla \cdot (\varepsilon \nabla \psi) = -\rho \quad (5)$$

where  $\varepsilon_0$  is the vacuum permittivity and  $\varepsilon$  is the dielectric constant of the medium. When there are ions involved, the volumetric charge density can be written as:

$$\rho = e \sum_i z_i c_i \quad (6)$$

with  $e$  as the elementary charge,  $z_i$  and  $c_i$  as the charge and concentration of the ion  $i$ , respectively.

By applying the Boltzmann distribution to represent the ion concentration and considering the dielectric constant uniform throughout the space, the following Poisson-Boltzmann equation (PBE) is obtained for a flat surface (LIMA, 2008):

$$\frac{d^2 \psi}{dx^2} = - \frac{e}{\varepsilon_0 \varepsilon} \sum_i z_i c_{i,0} \exp\left(\frac{-e z_i \psi}{k_B T}\right) \quad (7)$$

where  $c_{i,0}$  is the bulk concentration of ion  $i$ ,  $k_B$  is the Boltzmann constant and  $T$  is the temperature.

The Poisson-Boltzmann equation relates how the electrostatic potential varies with distance from a charged surface to bulk conditions of the medium. To solve the one-dimensional PBE, two boundary conditions are necessary to complete the system of equations, one at each boundary. Two boundary conditions normally used are:

$$\left. \frac{d\psi}{dx} \right|_{x=0} = - \frac{\sigma}{\varepsilon_0 \varepsilon} \quad (8)$$

$$\left. \frac{d\psi}{dx} \right|_{x \rightarrow \infty} = 0 \quad (9)$$

These are referred to as Neumann boundary conditions and they specify the derivative of the potential at the boundaries (CONSTANTINIDES; MOSTOUFI, 1999). For the first one, when  $x = 0$  (at the surface), the derivative of the potential is assumed to be equal to the surface charge density ( $\sigma$ ) of the object studied, in the case of this work, the surface of the yeast cell. For the second boundary condition, when  $x \rightarrow \infty$  (far away from the surface), we assume that the derivative is equal to zero, which means that there is no more variation of the potential and properties reach bulk values.

### 1.3 Poisson-Boltzmann equation with fixed charges

In some cases, fixed charges can be included in the system studied, e.g., proteins and other charged macromolecules that are present in specific positions. To account for the impact of these charges, a term can be added into the Poisson-Boltzmann equation, describing the charge density of the fixed charges. The modified Poisson-Boltzmann equation that accounts for the presence of fixed charges is (BARBOSA; LIMA; TAVARES, 2015):

$$\frac{d^2\psi}{dx^2} = - \frac{e}{\varepsilon_0 \varepsilon} \sum_i z_i c_{i,0} \exp\left(\frac{-e z_i \psi}{k_B T}\right) - \rho_f \quad (10)$$

The term that represents the fixed charges ( $\rho_f$ ) can be a number if the charge density is constant or it can be a function that describes the fixed charge profile throughout the space, if it varies with any given parameter.

This equation can be useful for systems that are made of a thick and permeable surface/membrane, where instead of the charges being all present on the boundary of a surface, they are spread out over the thickness of the penetrable surface. For the case of a penetrable surface with a considerable thickness inserted in a medium, the boundary conditions appropriate for the resolution of the Poisson-Boltzmann equation with fixed charges are (BARBOSA; LIMA; TAVARES, 2015):

$$\left. \frac{d\psi}{dx} \right|_{x \rightarrow -\infty} = 0 \quad (11)$$

$$\left. \frac{d\psi}{dx} \right|_{x \rightarrow \infty} = 0 \quad (12)$$

meaning that the potential stabilizes deep inside the permeable surface ( $x \rightarrow -\infty$ ) and far away from the surface ( $x \rightarrow \infty$ ), when properties reach bulk values of the medium. This last one is the same as for the Poisson-Boltzmann without fixed charges.

Despite of the boundary conditions necessary for resolution, in the case where the fixed charges are only present in one half of the domain, there are other two conditions that need to be satisfied as well. These conditions are shown in equations (13) and (14). They state that the potential and its derivative need to be equal at the center of the domain ( $x = 0$ ), the plane where the medium and penetrable surface meet. These conditions guarantee the continuity of the electrostatic potential (BARBOSA; LIMA; TAVARES, 2015).

$$\psi|_{x \rightarrow 0^+} = \psi|_{x \rightarrow 0^-} \quad (13)$$

$$\left. \frac{d\psi}{dx} \right|_{x \rightarrow 0^+} = \left. \frac{d\psi}{dx} \right|_{x \rightarrow 0^-} \quad (14)$$

By solving the Poisson-Boltzmann equation with or without fixed charges we obtain the electrostatic potential profile near a charged surface. Analyzing the results for the electrostatic potential over the domain of  $x$ , it is possible to obtain an estimate for the zeta potential of the particle. The zeta potential is a measurable parameter that can be obtained from electrophoretic experiments, and by comparing the calculated results to experimental results we can check for the accuracy of our calculations.

#### 1.4 Zeta potential

Most colloidal particles existing in natural waters and industrial effluent streams have negative charged surfaces and the stability of these particles can change depending on

solution pH, ion concentration among other factors. The stability of colloidal particles is usually investigated in terms of the zeta potential, as it is a widely used experimental measure that can help to characterize the double layer of particles (NARONG; JAMES, 2006). In this experiment the use of electrolyte solutions as a polarizable solvent is necessary (NANOCOMPOSIX, c2020)

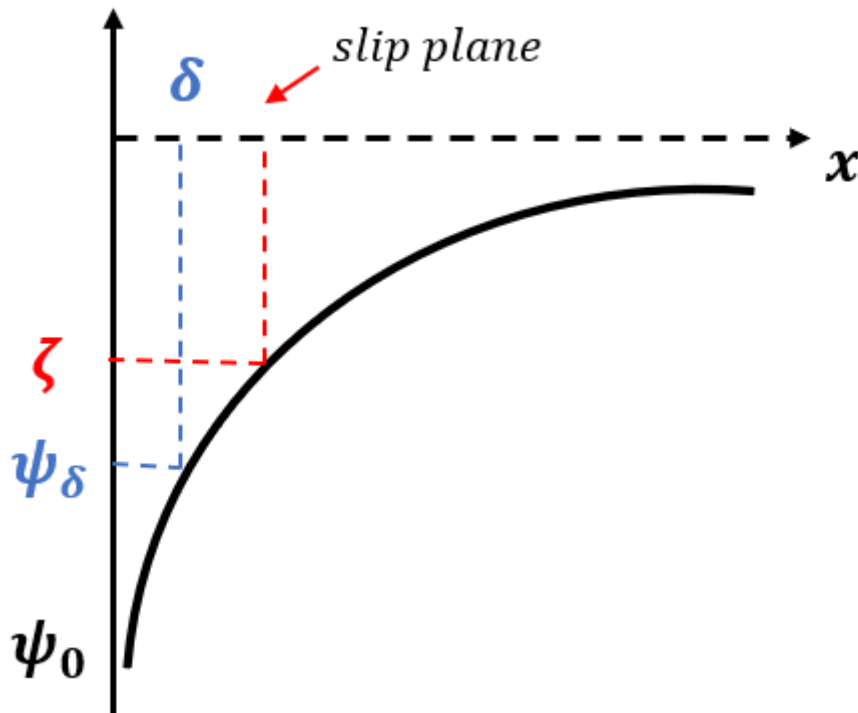
The zeta potential is a key parameter in a variety of biological applications, such as, characterization of biomedical polymers, membrane separation, mineral processing, water treatment, protein separation and purification, among others (SALGIN S.; SALGIN U.; BAHADIR, 2012).

The zeta potential is a parameter that is obtained from experimental electrophoretic mobility data by using equations that correlates both. For large particles like biological cells, the Helmholtz-Smoluchowski equation is the most used. Regarding the mobility of particles, when a colloidal particle moves it carries along with it a layer of ions attached on its surface that moves with the same velocity as the particle. The location of this moving surface is called the slipping plane and the value of the electrostatic potential at this plane is referred as the zeta potential (OHKI; OHSHIMA, 1995).

Figure 2 shows how the electrostatic potential is expected to vary with distance from a charged surface. The liquid layer surrounding the particle is usually divided into two regions: the Stern layer ( $\delta$ ) which is the layer where are located the ions that are adsorbed to the surface, and the diffuse layer ( $\kappa^{-1}$ ) where the ions are less firmly attached to the particle (SALGIN; SALGIN; BAHADIR, 2012). Located somewhere in between the extent of those two regions is where lies the slipping plane, where the zeta potential is measured ( $\zeta$ ). In this way, the value of the zeta potential is expected to be smaller in magnitude than the value of the potential at the Stern plane ( $\psi_\delta$ ), that for its turn is smaller than the value at the surface ( $\psi_0$ ) (OHKI; OHSHIMA, 1995).

A challenging task in dealing with biological surfaces is where to consider the distance of the slipping plane. For smooth particles, the location of this plane is usually close to the Stern plane, but for some biological surfaces containing different groups of macromolecules the location of this plane is not well define and it can extend quite a distance from the surface (OHKI; OHSHIMA, 1995).

Figure 2 - Components of the electrical double layer



Source: The author, 2020.

For the *S. cerevisiae* yeast cell many zeta potential experimental data are available in the literature (AMORY; ROUXHET, 1988; NARONG; JAMES, 2006; THONART; CUSTINNE; PAQUOT, 1982; SCHWEGMANN; FEITZ; FRIMMEL, 2010). Analyzing some works, one experiment that stood out was the experiment of Narong and James (2006) in which they measured the zeta potential of *S. cerevisiae* for two different ionic concentrations of NaCl (1 mM e 10 mM) in a range of pH values varying from 3.0 to 10.0 – 8 experimental points were obtained for each ionic concentration. These data are used later in Chapter 3 for comparison with the results calculated using theoretical models.

### 1.5 Parameter estimation

Parameter estimation methods are techniques that estimate values of parameters based on measured experimental data. One of the most common methods for estimating parameters is the least-squares fitting, in which the parameters ( $\theta_j$ ) are estimated by minimizing the

squared difference between experimental values ( $y_{exp_i}$ ) and values predicted by the model ( $y_{model_i}$ ) (ZHAO et al., 2015). The objective function of least-squares method can be seen in equation (15).

$$F_{obj}(\theta_j) = \sum_i^{N_{exp}} (y_{exp_i} - y_{model_i}(\theta_j))^2 \quad (15)$$

where  $N_{exp}$  is the total number of experimental data;  $y_{exp}$  are the experimental variables and  $y_{model_i}(\theta_j)$  are the variables calculated by the model using the parameters  $\theta_j$ .

To minimize the objective function ( $F_{obj}$ ) an optimization method is necessary, as for example, the sequential least squares programming and the Nelder-Mead simplex (BOGGS; TOLLE, 1995; NELDER; MEAD, 1965).

Both methods are deterministic, available in the Scipy library of Python, and can be used in solving nonlinear problems. Each of the methods have different features that are of interest in this study: the sequential least squares programming algorithm uses both the first and second derivative of the function and is a method for constrained optimization, while the Nelder-Mead simplex algorithm does not require the use of any derivatives but it is a method that does not admit any constrains. Because it uses derivatives and admits constrains, the sequential quadratic programming is an optimization method that finds the solution much faster than the Simplex method, nevertheless on situations where we can encounter problems obtaining the derivatives of the function, the Simplex method is a better option.

## 1.6 Parameter analysis methods

### 1.6.1 Monte Carlo method

One method that can be used for parameter estimation and analysis is the Monte Carlo method (CHO et al., 2003). This method is based on calculating values of the model or objective function using many random sets of parameters. By analyzing its results it is possible to infer which region seems to have the best sets of parameters for the model studied.

Despite being theoretically simple, this method can provide valuable information on how the parameters are related to the model. However, because this method provides information by mapping out random regions, many calculations are performed during the application of the method, and the computational effort required may be elevated.

### 1.6.2 Sensitive parameter analysis

The matrix of the derivatives of the model in relation to the parameters is called the sensitivity matrix ( $S_{i,j}$ ) (BATZEL; BACHAR; KAPPEL, 2013).

$$S_{i,j} = \frac{dy_i}{d\theta_j} \in \mathbb{R}^{ixj} \quad (16)$$

with  $y_i$  being the variable calculated by model at point  $i$ , and  $\theta_j$  being the parameter  $j$  in the set of parameters of the model. For better analysis of the sensitivity matrix, especially if the parameters analyzed have different orders of magnitude, we can normalize the sensitivity matrix by multiplying each derivative by  $\theta_j/y_i$ .

This matrix can provide information on the most sensitive and the least sensitive parameters, with the most sensitive parameters being the one that most influence the model and least sensitive the ones that have little influence in the model's results.

An easy and effective way to analyze the parameters using this matrix is to perform a QR decomposition on it (DEUFLHARD; ROBLITZ, 2015). The QR decomposition is a method that divides the original matrix into two new matrices easier to analyze (Q and R), besides obtaining the decomposed matrices this decomposition can also be performed with the additional features of column pivoting and rank determination that are very helpful in the sensitive parameter analysis.

The rank number of a matrix indicates the number of columns that are independent and column pivoting of the matrix rearranges the order of the columns of the matrix R from the one with the biggest norm to the one with the smallest. This is helpful because by analyzing the rank of the sensitivity matrix it is possible to determine if all parameters are independent or if there is any dependency among them. Moreover, the columns pivoting can

indicate the most sensitive parameters (highest norm) and least sensitive ones (lowest norm) (DEUFLHARD; ROBLITZ, 2015).

In Scilab software it is possible to find an implemented algorithm for the QR decomposition with the additional features of column pivoting and rank determination.

## 2 MODEL AND METHODS

### 2.1 Yeast surface charge regulation function

To be able to calculate the electric potential near the yeast cell wall it is essential to know the surface charge of the cell. As shown in Section 1.1, the structures responsible for the cell surface charge are the ionizable functional groups present on the cell wall, so, in order to calculate the total charge on the cell surface, it is necessary to take into account the contribution these groups.

Considering that the groups can be in their ionized form or not, the total amount of basic ( $N_b$ ) and acidic ( $N_a$ ) groups are:

$$N_a = C_{AH} + C_{A^-} \quad (17)$$

$$N_b = C_{BH^+} + C_B \quad (18)$$

The surface groups that contribute to the cell surface charge are the ones in their ionized state, acidic groups that lost a proton and basic groups that gained one, so it is important to know which groups are ionized and which are not.

A previously mentioned parameter that can describe the ionization rate of the functional groups is the dissociation constant ( $K_a$ ), the relations for the  $K_a$  of basic and acidic groups can be seen in equations (3) and (4). It should be noted that the dissociation constant is a function of the local proton concentration at the surface ( $C_{H_s^+}$ ) which in its turn is influenced by the surface charge. Due to the surface charge influence, the local concentration of protons is expected to follow the Boltzmann distribution and it can be expressed as a function of the electrostatic potential as:

$$C_{H_s^+} = C_{H_{Bulk}^+} \exp(-e\psi_s/k_B T) \quad (19)$$

where  $\psi_s$  is the electrostatic potential at the surface, and  $C_{H_{Bulk}^+}$  is the bulk concentration of  $H^+$ .

By combining equations (3), (4), (17), (18) and (19), and rearranging them to obtain a function of number of groups ( $N_a$  and  $N_b$ ), dissociation constants ( $K_{a\_ac}$  and  $K_{a\_bas}$ ), and bulk proton concentration  $C_{H_{Bulk}^+}$ , or pH, the following function is obtained (POORTINGA et al., 2002):

$$\frac{\sigma}{e} = \sum_l \frac{N_{b,l} C_{H_{Bulk}^+} \exp\left(\frac{-e\psi}{k_B T}\right)}{C_{H_{Bulk}^+} \exp\left(\frac{-e\psi}{k_B T}\right) + K_{a\_bas,l}} - \sum_k \frac{N_{a,k} K_{a\_ac,k}}{K_{a\_ac,k} + C_{H_{Bulk}^+} \exp\left(\frac{-e\psi}{k_B T}\right)} \quad (20)$$

where the subscript  $l$  refers to the basic sites of type  $l$ , whereas  $k$  is related to the acidic sites of type  $k$ .

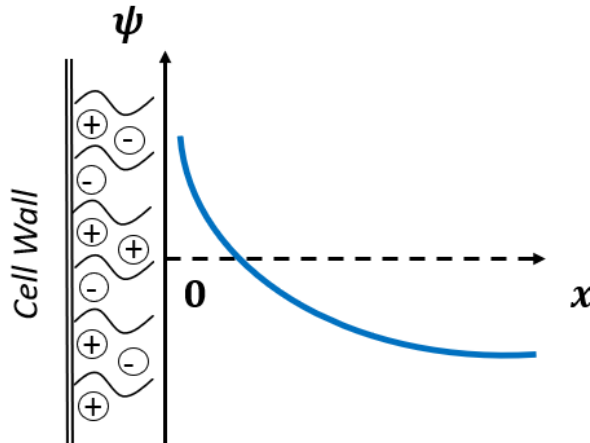
The parameters selected to represent the charge surface function were chosen due to the fact that they can be either measured or calculated using other measurable parameters. Potentiometric titration experiments can provide values on both the dissociation constant and the amount of ionizable sites available (HONG; BROWN, 2006; ZHANG et al., 2010).

## 2.2 Charge regulation on the surface model

Considering the yeast cell wall a charged surface that is impenetrable by ions, when yeast cells are inserted in a medium containing ions the Poisson-Boltzmann equation can be used to describe its electrostatic potential.

By combining the Poisson-Boltzmann equation and boundary conditions described in equations (7), (8) and (9) with the yeast surface charge function presented in equation (20), the charge regulation on the surface model is obtained. In this model, the surface charge function enters in the place of the surface charge density ( $\sigma$ ) in the boundary condition in equation (8), the one at the surface. In Figure 3 is possible to see a drawing of the electrostatic potential described by this model, this illustration will be useful for comparison to the expected profile of the volumetric charge density model.

Figure 3 – Expected curve of the electrostatic potential for the charge regulation model



Source: The author, 2019.

The denomination “charge regulation” in the model is related to the fact that both the surface charge function and the PBE are functions of the electrostatic potential, and therefore they need to be solved simultaneously (HONG; BROWN, 2008).

To solve the model the finite volume method was used. This method is based on physical laws and relies on linear approximations of the differential equation (LIMA; TAVARES; BISCAIA JR, 2007). More about the finite volume method can be seen in appendix A.

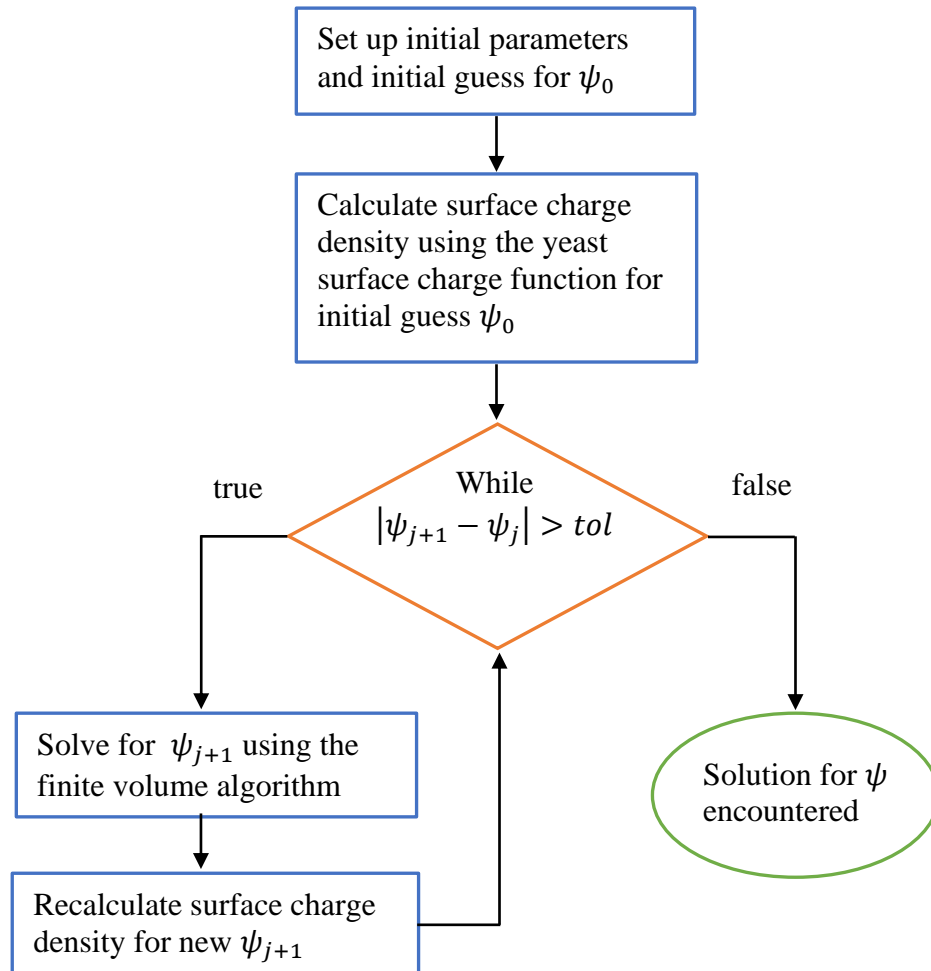
Figure 4 summarizes the algorithm for the resolution of the model. It starts by setting up the initial parameters which can be divided into three sections: parameters of the model, of the method and of the functional groups. The parameters of the model are temperature ( $T$ ), dielectric constant of the medium ( $\epsilon$ ), initial and final position ( $x_0$  and  $x_f$ ), bulk concentration of ions ( $C_{i0}$ ), valency of ions ( $z_i$ ) and pH.

The parameters for the numerical method are number of volumes ( $n$ ) and tolerance ( $tol$ ). Finally parameters of the cell wall functional groups are number of acid functional groups ( $N_{a,k}$ ), number of basic functional groups ( $N_{b,l}$ ), dissociation constant of acid functional groups ( $K_{a,ac,k}$ ) and dissociation constant of basic functional groups ( $K_{a,bas,l}$ ).

After setting up initial parameters, the next step is to propose an initial guess for the vector of electrostatic potential profile ( $\psi_0$ ) near the cell wall. For this vector it was assumed a linear variation from  $\psi_1$  at the surface (initial position) to 0 mV at the bulk (final position), where  $\psi_1$  is an expected value taken from the literature. With the initial guess for the

electrostatic potential an initial surface charge density is calculated, and the program is ready to enter the finite volume method.

Figure 4 – Algorithm for the charge regulation model



Source: The author, 2020.

Entering the finite volume method, it calculates new electrostatic potential profile at each iteration until the “while criterium” is met, which refers to norm of the vector for the electrostatic potential of the latest iteration minus the one of the previous iteration being smaller than the defined tolerance (tol) of the method. Furthermore, with each iteration and new potential calculated, the surface charge densities need to be updated, due to their dependency. When the while criterium is satisfied the method converges and the final value for the electrostatic potential is obtained.

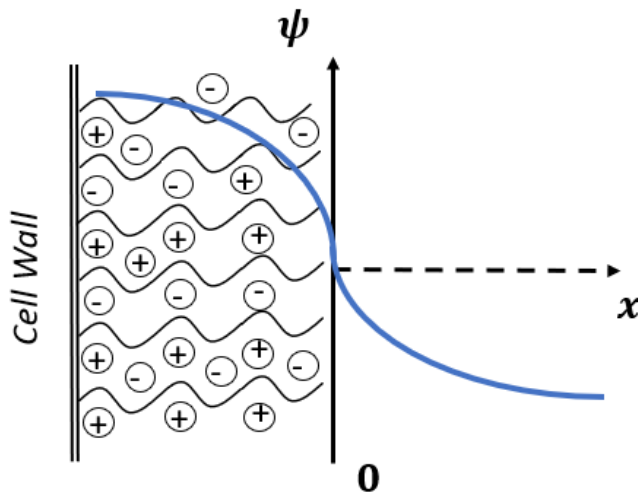
The algorithm for the charge regulation model was validated using data and results for the *E. coli* and *B. brevis* bacteria from the work of Hong and Brown (2008).

### 2.3 Charge-regulated volume charge density model

Considering the yeast cell wall a penetrable layer with a considerable thickness, a more appropriate equation to describe its electrostatic potential profile is the Poisson-Boltzmann equation with fixed charges (POORTINGA et al., 2002). If the cell wall has a significant thickness than it is possible to assume that the functional groups are spread out over the volume of the cell wall, and, in the case where ions can penetrate this layer and cause variation of the charge inside the cell wall, the charges of the functional groups are better described as fixed charges in the space of the penetrable cell wall (POORTINGA et al., 2002).

Figure 5 illustrates the expected electrostatic potential profile considered by the volumetric charge density model. Comparing Figure 5 to Figure 3 from the previous model, we can see that now the electrostatic potential is allowed to vary inside the cell wall.

Figure 5 – Expected electrostatic potential for the volumetric charge density model



Source: The author, 2019.

In this model, the yeast surface charge function described by equation (20) enters not as a surface charge density in a boundary condition, but as volumetric charge density ( $\rho_f$ ) in the Poisson-Boltzmann equation with fixed charges described by equation (10). For surfaces with a significant thickness, this equation can be solved with the use of the boundary conditions presented in equations (11) and (12).

Because the fixed charges in this case are only present in one part of the domain, the function that describes the fixed charges ( $\rho_f$ ) is discontinuous over the spatial domain. To

solve for the electrostatic potential in the space of the cell wall and the medium together we need to ensure the continuity of the electrostatic potential mentioned in equations (13) and (14). In the work of Barbosa, Lima and Tavares (2015) that used the charge-regulated volumetric charge density model to calculate the electrostatic potential on the *B. brevis* bacterial surface, the use of smoothing function was made to guarantee continuity over the transition of the regions.

In this work, the same smoothing function used by Barbosa, Lima and Tavares (2015) was used to calculate the electrostatic potential on the *S. cerevisiae* yeast cell wall. The function used is base on the hyperbolic tangent of the spatial domain and it is presented in equation (21).

$$v(x, \eta) = \frac{1 + \tanh\left(\frac{x - x^*}{\eta}\right)}{2} \quad (21)$$

The parameter  $\eta$  is related to the smoothness of the function, and  $x^*$  indicated the point of transition between the two regions. The way this function makes a smooth transition from one region to another is the following:

$$\rho_f(x, \eta) = v(x, \eta)\rho_{region1} + [1 - v(x, \eta)]\rho_{region2} \quad (22)$$

In this function, when  $x$  is smaller than  $x^*$  the function of the fixed charges is activated ( $\rho_{region2}$ ), and when  $x$  is greater than  $x^*$  another function of the fixed charges is activated ( $\rho_{region1}$ ). In the case of the system studied, the function activated when  $x$  is smaller than  $x^*$  is the yeast surface charge function, but for  $x$  greater than  $x^*$  there is no function to be activated since the medium does not possess fixed charges. Consequently, the function of  $\rho_f$  for the system here studied is reduced to:

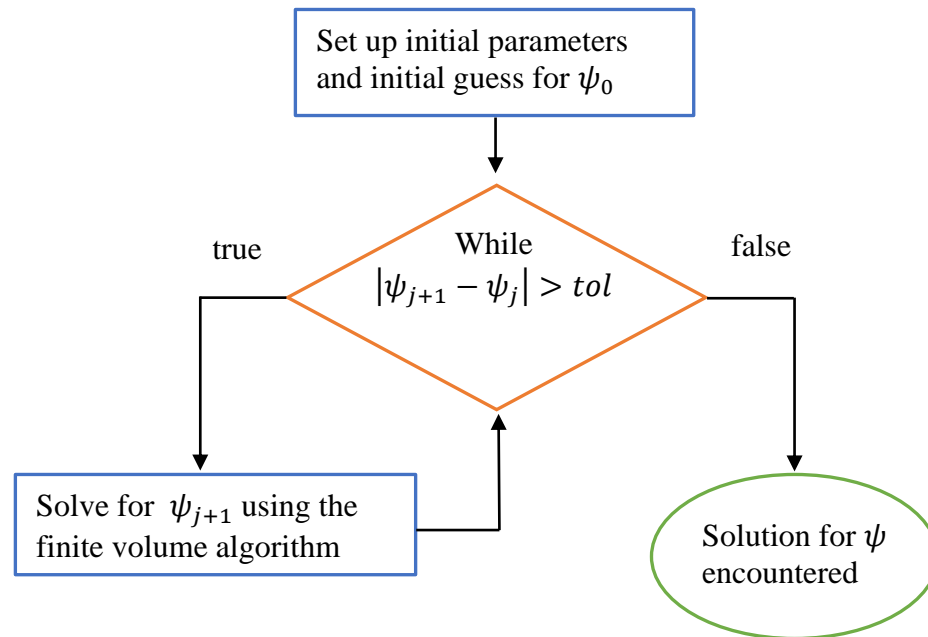
$$\rho_f(x, \eta) = (1 - v(x, \eta))\rho_{yeast\ cell\ wall} \quad (23)$$

The algorithm for solving this model is not so different from the one for the charge regulation model as demonstrated by Figure 6. The difference between them is that in the solution for the volumetric charge density model it is not necessary to recalculate the surface charge density in every iteration, since the surface volumetric charge density is solved

together with the potential in the PBE for this model. The initial parameters and initial guess for the electrostatic potential ( $\psi_0$ ) used for this model were the same as the ones described for the charge regulation model with the only difference in the unit of the number of groups parameters ( $N_{a,k}$  and  $N_{b,l}$ ) that are now given in number of groups per unit of volume instead of area.

The method used in solving the model was once again the finite volume method, and criterium and tolerance for convergence of the method were also the same as in the surface charge regulation model.

Figure 6 – Algorithm for the volumetric charge density model



Source: The author, 2020.

The algorithm for the charge regulated volumetric charge density model was validated using data and results for the *B. brevis* bacteria from the work of Barbosa, Lima and Tavares (2015).

## 2.4 Parameters of the model

In the resolution of the model, some parameters were kept fixed, while others could vary. In this section we will comment and explain the values of some parameters.

First, it's worth mentioning that when solving the finite volume method it is a good practice to write all parameters and variables in a dimensionless form, so before starting the method we made sure to make all variables dimensionless.

The parameters that were kept fixed during the calculations can be seen in Table 1. Commenting on the value of a few parameters, since the goal of this study was to compare results of the model with experimental ones, the conditions in the calculations needed to be the same as the conditions used in obtaining the experimental results. The experimental zeta potential data of Narong and James (2006) were obtained in a medium composed of water and different concentrations of salt (NaCl) at room temperature at 25 °C. Hence, it was necessary to set up the parameters  $z_i$ ,  $T$  and  $\varepsilon$  according with these conditions.

It is also worth pointing out that the values of  $x_0$  and  $x_f$  in Table 1 are in terms of the Debye length and they are dimensionless. The value chosen for  $x_f$  is one where we expect properties to reach bulk values. The value for the parameter  $\eta$  used was taken from the work of Barbosa, Lima and Tavares (2015).

For the parameters of the numerical method the tolerance was fixed in  $10^{-7}$  and the number of volumes ( $n$ ) used for each model was one that guaranteed grid convergence for the bulk ionic concentration of 1 mM (case with longest x vector). For grid convergence, we looked at the value of the electrostatic potential at the stern layer, it was considered converged when the difference of the values with change in  $n$  was smaller than 0.1.

Table 1 – Fixed parameters of charge regulation model

Model's parameters:	
$z_i$	[1, -1]
$\varepsilon$	78.5
$T$	298.15 (K)
$x_0$	0
$x_f$	5
$\eta$	0.1

Numerical method parameters:	
$n$ ( <i>charge regulation</i> )	300
$n$ ( <i>volumetric charge density</i> )	600
$tol$	$1 \times 10^{-7}$

Source: The author, 2020.

Some parameters that were allowed to vary and are worth mentioning due to their importance and influence in the results of both models are the functional groups parameters. The number and the dissociation constant of each functional group are necessary to characterize the cell surface and these parameters can be obtained through potentiometric titration experiments. Since experiments were not performed during this work, a literature review was carried out to find experimental potentiometric titration data for the *S. cerevisiae* yeast cell.

Several potentiometric titration experiments for the *S. cerevisiae* yeast cell have been reported, mainly for works involving the study of its electrophoretic behavior and heavy metal biosorption. A few studies identified 3 groups on the cell wall (PARVATHI; NARESHKUMAR; NAGENDRAN, 2007; DI CAPRIO et al., 2014), but more reports showed 4 groups present on the yeast cell wall (NAEEM; WOERTZ; FEIN, 2006; ZHANG et al., 2010; LIU et al., 2017; ROGOWSKA et al., 2018). Analyzing experiments conditions and results of all studies, we concluded that the work of Zhang et al. (2010) would be the best to characterize the yeast cell surface. Their experimental results for the *S. cerevisiae* yeast cell identified 4 groups on the cell surface (carboxyl, phosphoryl, hydroxyl and amine) and determined the dissociation constant ( $pK_a$ ) and site density for each group. These results can be seen in Table 2.

In order to be applied into the models these data have to be treated, e. g., for the case of the  $pK_a$ , only one value can be incorporated in our calculations, so a specific value for each functional group in the ranges reported in Table 2 has to be chosen or estimated.

Table 2 – Potentiometric titration data of *S. cerevisiae*

<b>Groups:</b>	<b><math>pK_a</math></b>	<b>Site density (mmol/g)</b>
<b>Carboxyl</b>	3.52 – 5.34	$0.45 \pm 0.07$
<b>Phosphoryl</b>	6.24 – 7.30	$0.35 \pm 0.04$

<b>Amine</b>	8.86 – 10.92	$0.25 \pm 0.02$
<b>Hydroxyl</b>	9.47 – 10.13	$0.85 \pm 0.01$

---

Source: ZHANG et. al, 2010.

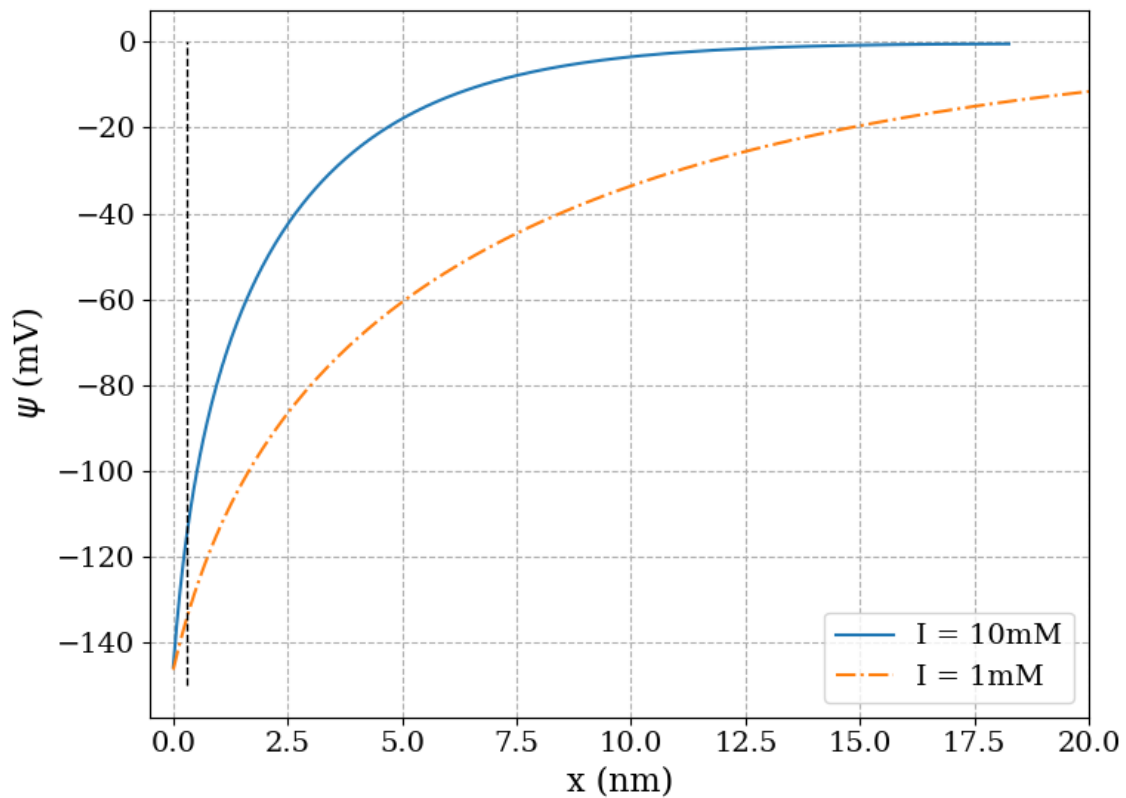
In relation to the site density, this value was used to calculate the model's required parameter that is the number of groups (per area or volume). For this calculation, data of cell weight and surface area/volume for the *S. cerevisiae* yeast cell are also necessary. In the work of Klis et al. (2014) it is possible to find information on the weight and dimension of the *S. cerevisiae* yeast cell. Data for the *S. cerevisiae* haploid cell indicates that its biomass dry weight is of 16.5 pg, its surface area is 60  $\mu\text{m}^2$  and the thickness of the cell wall appears to be of 115 nm at late exponential phase cells.

### 3 RESULTS AND DISCUSSION

#### 3.1 Charge regulation on the surface

The first results for charge regulation applied to the surface model described in the previous chapter can be seen in Figure 7. They refer to pH 7.0 and ionic strengths of 10 mM and 1 mM (NaCl). The functional groups parameters used in the calculations are displayed in Table 3, they were obtained based on the potentiometric titration data available Table 2.

Figure 7 – Electrostatic potential of the *S. cerevisiae* yeast cell wall calculated by the charge regulation on the surface model at pH=7.0.



Legend: The dashed black line represents the Stern layer.  
Source: The author, 2020.

Table 3 – Functional groups parameters

	<b>Carboxyl</b>	<b>Phosphoryl</b>	<b>Hydroxyl</b>	<b>Amine</b>
<b>pK<sub>a</sub></b>	4.43	6.77	9.80	9.89
<b>N (#/nm<sup>2</sup>)</b>	74.50	57.94	140.7	41.39

Source: The author, 2019.

In Table 3, for the dissociation constant (pK<sub>a</sub>) parameters the average values of the respective reported range for each group were used, the number of groups (N) were calculated using the site density values of Table 2 together with data of cell weight (16.5 pg) and surface area (60 μm<sup>2</sup>) of *Saccharomyces cerevisiae* haploid cell, taken from Klis, de Koster and Brul (2014).

Observing Figure 7 we can see how the potential varies for different ionic strengths. Both curves show relatively close surface potential values, it appears that for this system and ionic strengths tested, the ionic strength does not have much influence on the value of potential at the surface. From there on, the curve decline for 10mM is faster than for 1mM and they show different electrostatic potential results for all distances from the surface. The calculated surface potential is around of -146 mV. Analyzing the model's values at the Stern layer (layer of adsorbed ions), considered here to be of 0.3 nm of distance (one hydrated ion diameter) and indicated in Figure 7 by the black dashed line, we find that the potential varies from -115 mV for 10 mM to -134 mV for 1 mM, decreasing in magnitude with increasing ionic strength.

An important measure in colloidal systems is the zeta potential, which is the value of the electrostatic potential at the so-called slipping plane. According to the definition of slipping plane, the ions and molecules located closer the surface than this plane are bind to surface and move with the same velocity as the particle. The exact location of this plane is unknown, but it is usually a few Å away from the surface for smooth particles (OHKI; OHSHIMA, 1995). A commonly used approximation for the zeta potential in mathematical models is the potential at the Stern plane (HONG; BROWN, 2008; BARBOSA; LIMA; TAVARES, 2015). In this work the Stern potential will be used in comparisons with experimental zeta potential results.

Comparing the model's results with experimental zeta potential of the *S. cerevisiae* yeast cell reported by Narong and James (2006) we can observe that the results are quite different: while the experimental zeta potential values at pH 7.0 are around -15.4mV and -26.3mV for ionic strength of 10mM and 1mM respectively, the model predicts much more

negative potential values, about 100mV more negative. A possible explanation for the disparity of these results could be related to the structure of the yeast cell surface. The yeast cell surface is not a smooth surface, instead its complex surface composed by a layer of macromolecules containing ionizable groups, and because this layer can have a significant thickness, the charges on this surface are most likely distributed over the extent of this layer. Taking this into consideration, Hong and Brown (2008) supposed that only the groups on the most outer surface of this layer would affect the cell surface charge, and to compensate for this effect, they proposed the use of an effectiveness coefficient ( $\lambda_{eff}$ ) to correct the total number of groups present on the surface.

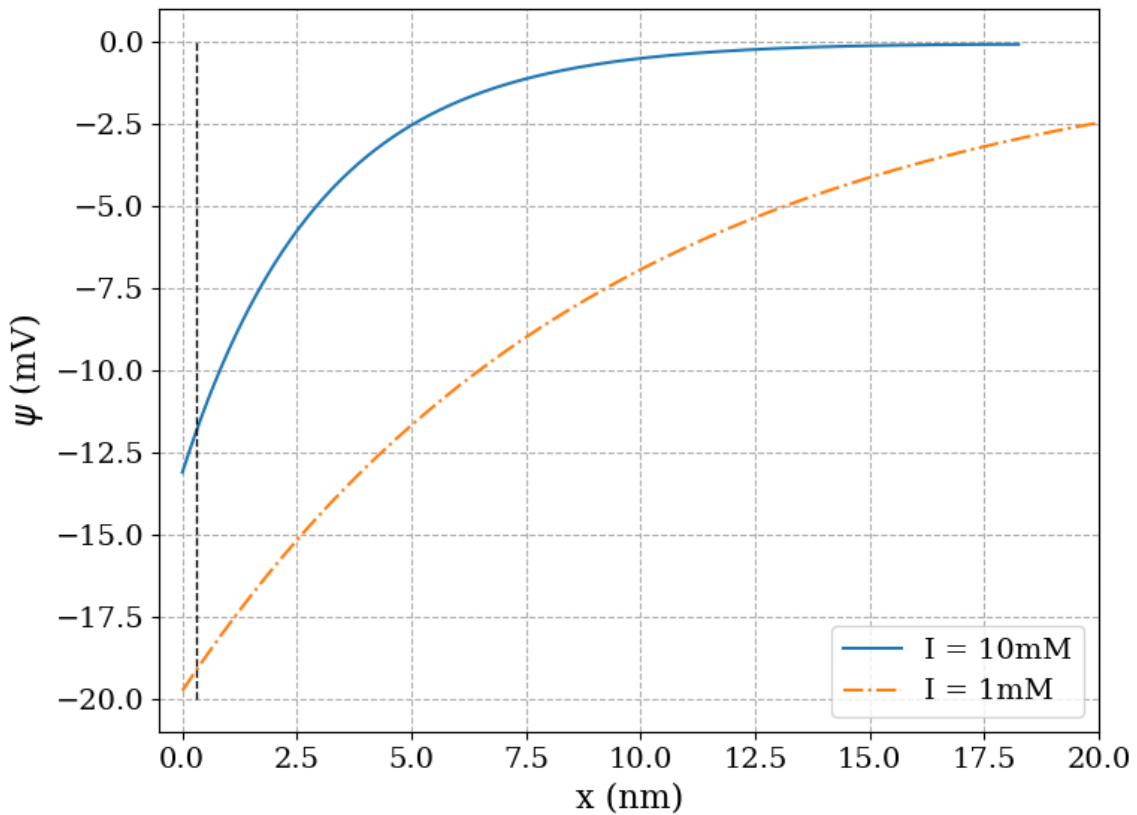
$$N_i^{eff} = N_i \lambda_{eff} \quad (24)$$

By inserting this coefficient into the model and calculating the surface charge for the effective number of groups ( $N_i^{eff}$ ) better results are expected to be achieved. To find a good value for this parameter ( $\lambda_{eff}$ ), an estimation was performed using the least-squares method that compared our model potentials at the Stern layer with the experimental zeta potential results of Narong and James (2006) over a range of pH (3 – 10). One effectiveness coefficient was estimated for each ionic strength (10 mM and 1 mM) as it has been shown to vary with ionic strength (HONG; BROWN, 2008). The functional groups parameters used were the ones in Table 3 and the optimization algorithm used to solve the estimation problem was the Nelder-Mead Simplex algorithm implemented in the Python SciPy library.

Results of the estimation for initial guess of 0.5 returned effectiveness coefficients values of  $3.05 \times 10^{-4}$  for 10 mM and  $1.57 \times 10^{-4}$  for 1 mM. The order of magnitude is consistent with the ones encountered by Hong and Brown (2008) for the *E. coli* bacteria.

Results for the electrostatic potential calculated using the optimized effective number of groups can be seen in Figure 8, where it's visible that the calculated potential is a lot more compatible with experimental results. Electrostatic potential values at the Stern layer are -11.82mV and -19.08mV for 10 mM and 1 mM respectively, a deviation of 3 and 7 mV, respectively, from the experimental values. Because we are correcting the number of groups with a different coefficient for each ionic strength, results at the surface ( $x = 0$  nm) in Figure 8 are not as close as in Figure 7.

Figure 8 – Electrostatic potential of *S. cerevisiae* yeast cell calculated by the charge regulation on the surface model using the effective number of groups at pH=7.0

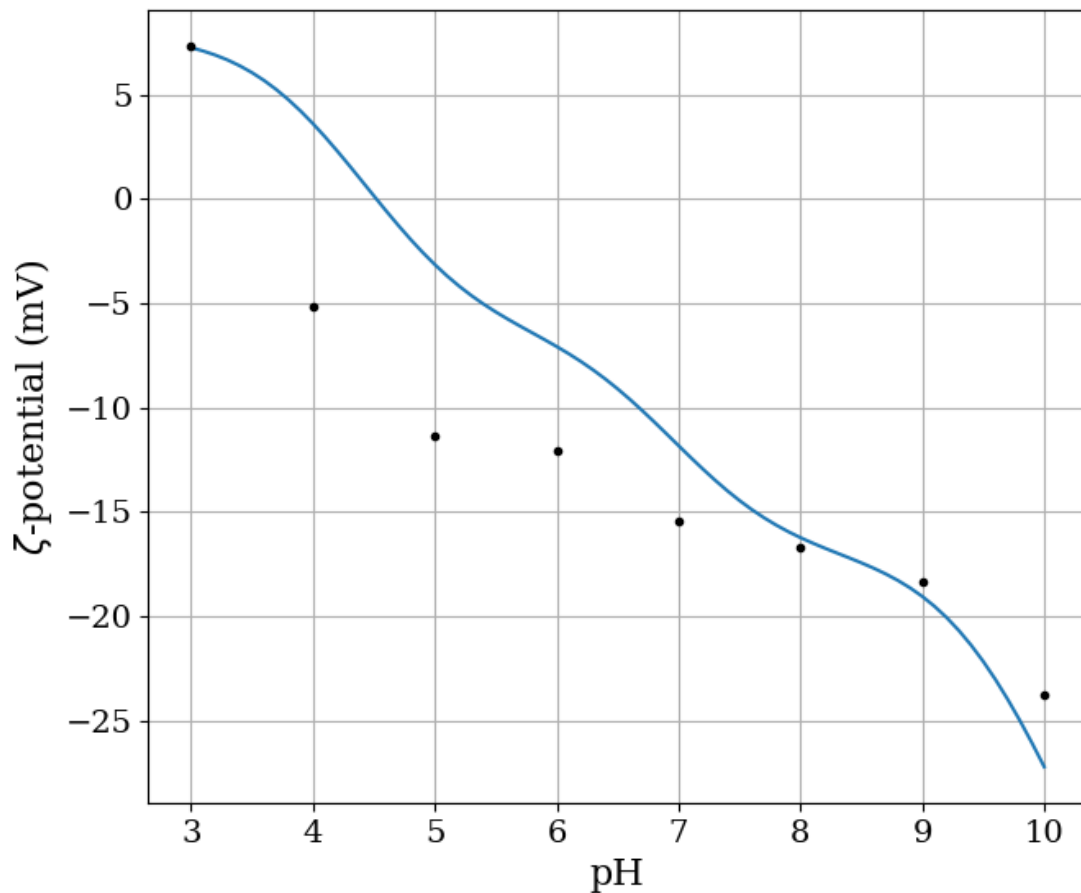


Legend: The dashed black line represents the Stern layer.  
Source: The author, 2020.

In Figure 9 we can see how zeta potential varies as a function of pH for ionic strength of 10 mM. Results of the charge regulation on the surface model using the effectiveness coefficient estimated previously ( $\lambda_{eff} = 3.05 \times 10^{-4}$ ) are represented by the curve; black dots represent the experimental results of Narong and James (2006).

Comparing the curve to experimental data, one can see that for basic pH values (8 - 10) the model can quantitatively reproduce experimental results, but for other points the model predicts lower values (in magnitude) for the potential than those experimentally measured, specially at pH 5.0, where the model's prediction is more than 10 mV different. For pH 3.0 the model matches the experimental result, but from there on the model cannot catch the quick drop that occurs in experimental values around pH 4.0 and 5.0.

Figure 9 – Modeled zeta potential of *S. cerevisiae* as a function of pH for 10 mM with effectiveness coefficient equal to  $3.05 \times 10^{-4}$

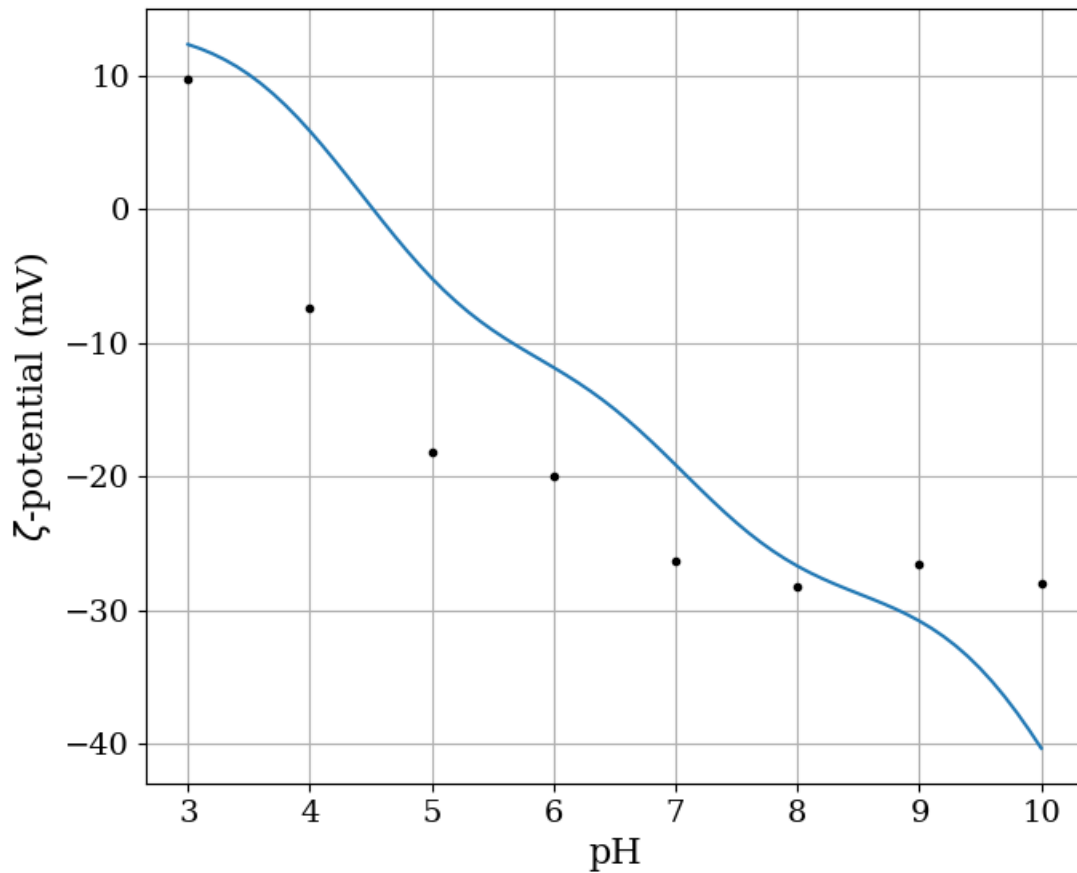


Legend: Modeled zeta potentials of *S. cerevisiae* are portrayed by the curve, whereas dots represent the experimental results of Narong and James (2006).  
Source: The author, 2020.

Figure 10 shows the model's zeta potential as a function of pH for ionic strength of 1 mM. Similar to Figure 9, the model was compared with experimental results of Narong and James (2006). The curve for 1 mM exhibits a similar shape to the one reported for 10mM, but unlike that curve, this one cannot describe the experimental results of basic pH values. For these concentrations, experimental zeta potential results exhibit an unexpected behavior: the potential seems to stabilize around a value (-26/-28mV) when it hits pH 8.0.

One hypothesis that could explain this behavior seen on experimental data is that there may be happening a saturation of ionizable sites around pH 8.0 for this ionic strength, implicating that probably all the surface available sites are already deprotonated when reaching pH 8.0, resulting on the potential hitting the most negative value it possibly can.

Figure 10 – Modeled zeta potential of *S. cerevisiae* as a function of pH for 1 mM with effectiveness coefficient equal to  $1.57 \times 10^{-4}$



Legend: Modeled zeta potentials of *S. cerevisiae* are portrayed by the curve, whereas dots represent the experimental results of Narong and James (2006).

Source: The author, 2020.

Looking at the curves of the model for both ionic strengths we can see that results do not provide a good fitting for experimental points. Considering this, the next step was to analyze the influence of other important parameters in the model: the dissociation constants ( $pK_a$ ). In Table 2 a range of values for the  $pK_a$  is provided and maybe other values in these ranges besides the ones chosen previously can better describe the system.

With that in mind it was decided to include the  $pK_a$  parameters in the parameter estimation procedure; therefore, a new parameter estimation was performed, this time for the effectiveness coefficient and the  $pK_a$  parameters. Estimations were carried out in similar conditions to the previous one for only the effectiveness coefficient. The  $pK_a$  parameters ranges of Table 2 were used as boundaries in the estimation. Because the Nelder-Mead algorithm does not accept boundaries, another algorithm had to be selected to solve the minimization problem, like the Sequential Least Squares Programming (SLSQP) algorithm

implemented in the Python SciPy. The initial guesses for the parameters were 0.5 for the effectiveness coefficient, and the average range values for the  $pK_a$  of each group that are displayed in Table 3. Results for the new parameter estimation are indicated in Table 4.

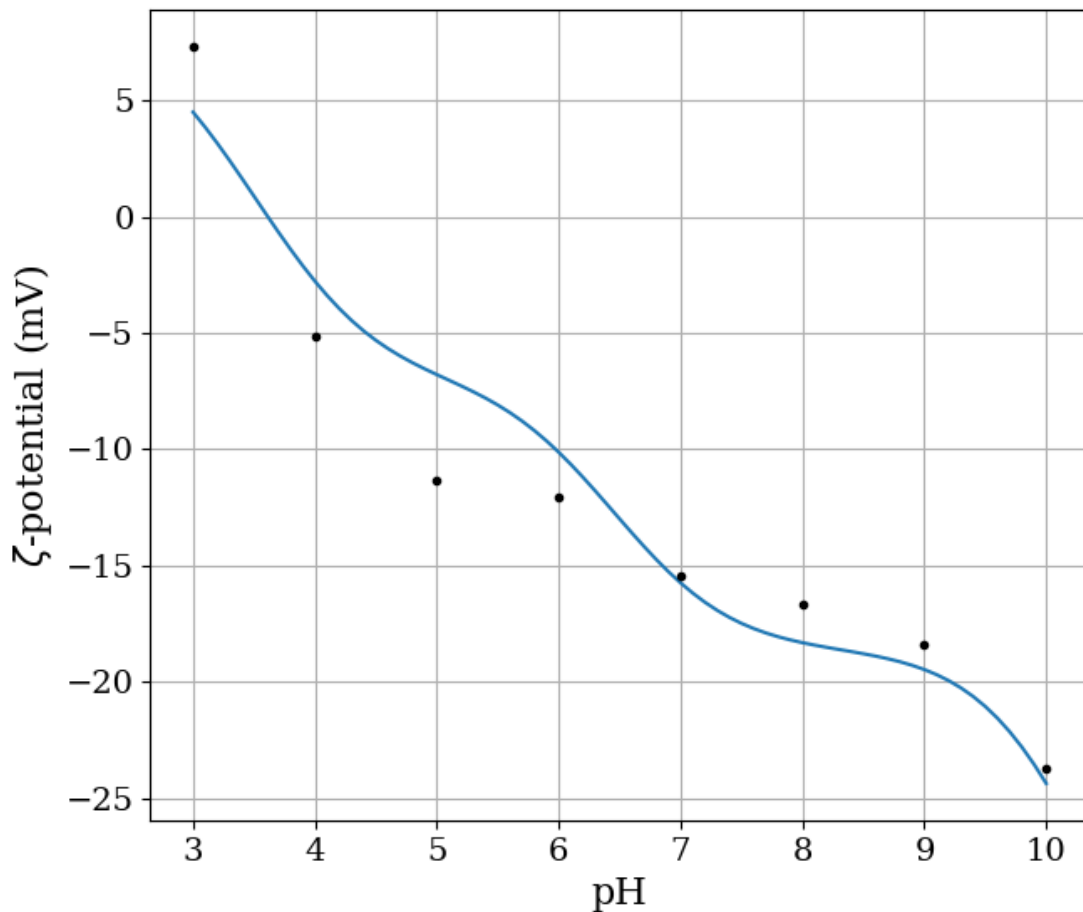
In Figure 11 one can see the results of the model with estimated parameters of Table 4 for 10 mM and, and in Figure 12, the results for 1 mM are displayed.

Table 4 – Estimated functional groups parameters (effectiveness coefficient and  $pK_a$ )

	$pK_{a,carboxyl}$	$pK_{a,phosphoryl}$	$pK_{a,hydroxyl}$	$pK_{a,amine}$	$\lambda_{eff}$
<b>10 mM</b>	3.52	6.24	10.13	10.92	$3.34 \times 10^{-4}$
<b>1 mM</b>	3.52	6.24	10.13	10.92	$1.54 \times 10^{-4}$

Source: The author, 2020.

Figure 11 – Modeled zeta potential for 10 mM with estimation of effectiveness coefficient and  $pK_a$



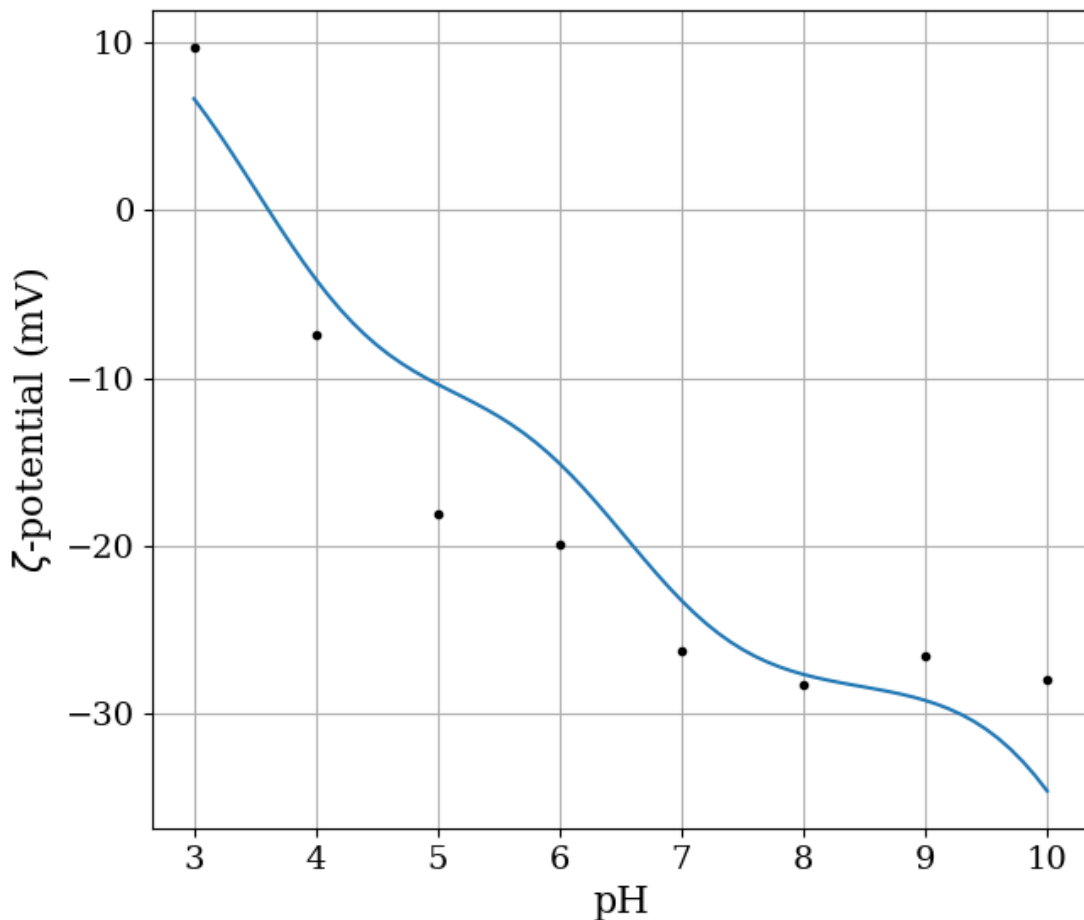
Legend: Modeled zeta potentials of *S. cerevisiae* are portrayed by the curve, whereas dots represent the experimental results of Narong and James (2006).

Source: The author, 2020.

It is possible to notice that for both curves the fitting has improved considerably. Specially from pH 3.0 - 7.0, curves for both ionic strengths got significantly closer to experimental points. When it comes to the decline that happens between pH 4.0 and 5.0, both curves still cannot capture that behavior and the potential at pH 5.0 is still the one with the largest error, 4.46 mV for 10 mM and 7.56 mV for 1 mM, while the mean errors to experimental points are of 1.9 mV for 10 mM and 3.7 for 1 mM.

For 10 mM, when the curve approached the points on the first half and middle of the curve, it ended up losing a bit of the fitting for higher pH values. The curve for 1 mM still does not describe the stagnation of the electrostatic potential that happens around pH 8.0. These observations reflect on the objective functions that for 10 mM the value found was of 41, whereas for 1 mM the value was of 164.

Figure 12 – Modeled zeta potential for 1 mM with estimation of the effectiveness coefficient and  $pK_a$



Legend: Modeled zeta potentials of *S. cerevisiae* are portrayed by the curve, whereas dots represent the experimental results of Narong and James (2006).

Source: The author, 2020.

Results for the effectiveness coefficient were not exactly the same as the ones encountered in the first optimization (only for the coefficient), but the values were relatively close.

Analyzing the results of the estimation in Table 4 it is possible to notice a common aspect in all estimated parameter: their values all lie in one of the boundaries specified when solving the estimation. This indicates that optimization with wider bounds can yield better results. With this in mind it was decided to carry out further research into the  $pK_a$  range of the functional groups present on the *S. cerevisiae* cell wall.

Research shows that the wider  $pK_a$  range encountered for the carboxyl group on microbial surfaces is between 2.0-6.0, for the hydroxyl group it is 8.0-12.0, for the amine group 9.0-11.0, while the phosphoryl group actually appears to have more than one dissociation constant, one at 0.2-2.9 and another at 5.6-7.2 (OHKI; OHSHIMA, 1995; HONG; BROWN, 2006; BARKLEIT; MOLL; BERNHARD, 2008). Table 5 shows the wider ranges encountered for  $pK_a$  of groups.

In the publication of Ohki and Ohshima (1995) it is possible to obtain further detailing on the  $pK_a$  of the biomolecules that these functional groups can be inserted in, explaining the extent of the ranges.

Table 5 – Wider  $pK_a$  range found in literature of the functional groups

<b>Groups:</b>	<b><math>pK_a</math></b>
<b>Carboxyl</b>	2.0 – 6.0
<b>Phosphoryl</b>	0.2 – 2.9; 5.6 – 7.2
<b>Amine</b>	9.0 – 11.0
<b>Hydroxyl</b>	8.0 – 12.0

Source: BARKLEIT; MOLL; BERNHARD, 2008. HONG; BROWN, 2006. OHKI; OHSHIMA, 1995.

Comparing this research to the values in Table 2, we can note that the amine group range seems compatible with the literature, while the ranges for the carboxyl and hydroxyl groups in Table 2 are a little narrower than the ones encountered on the research, and when it comes to the phosphoryl group, results in Table 2 are only accounting for the second  $pK_a$  of this group (5.6 - 7.2). If the phosphoryl groups present on the cell wall exhibits dissociation at its first  $pK_a$  (0.2 - 2.9), then maybe this contribution can be appearing on the first inflection point of the curve, together with the carboxyl group, explaining why the estimation returns lower values for the  $pK_a$  of the first group.

Considering all the reports on the ranges of the functional groups, it was decided to carry out another parameter estimation for the broader ranges encountered in the literature. For the carboxyl group it was used a range of 2.0 - 6.0, for the phosphoryl group 5.6 - 7.2 and for the hydroxyl group a range of 8.0 - 12.0. For the amine group the range in Table 2 is in more agreement with the wider ranges found in literature, for this reason it was not changed. The initial guess and minimization method used were the same as for the previous estimation.

Table 6 displays the results for the new estimation. For ionic strength of 10 mM, optimization with broader ranges achieved little difference regarding the first optimization. The  $pK_a$  of carboxyl was 3.51, very close to last estimation that yielded a value of 3.52; hydroxyl's  $pK_a$  went from 10.13 to 10.39, a slightly larger variation but also not very different; the  $pK_a$  of the phosphoryl group again landed on the lower boundary, that is now even lower, at a value of 5.6; and for the amino group,  $pK_a$  matched the new hydroxyl at 10.39 and left the boundary. The objective function had a considerable gain compared with the previous one, as it went from 41.97 to 32.09.

For the ionic strength of 1 mM, optimization with broader ranges appears to show more improvement. Commenting on the new  $pK_a$  results, the value for the carboxyl group again did not vary much from the previous value (3.52); for the phosphoryl group, once more the estimation threw the value for this group at the lower boundary of 5.6, decreasing the distance to the experimental points for pH 4.0 and 6.0 but still missing pH 5.0. Physically speaking, a high value like 12.0 is not expected for the  $pK_a$  of the hydroxyl group on the yeast cell wall. The  $pK_a$  of a group is not expected to change much with ionic strength and we can see that a high value as 12.0 was not obtained for ionic strength of 10 mM.

Table 6 – Results for optimization with broader  $pK_a$  ranges

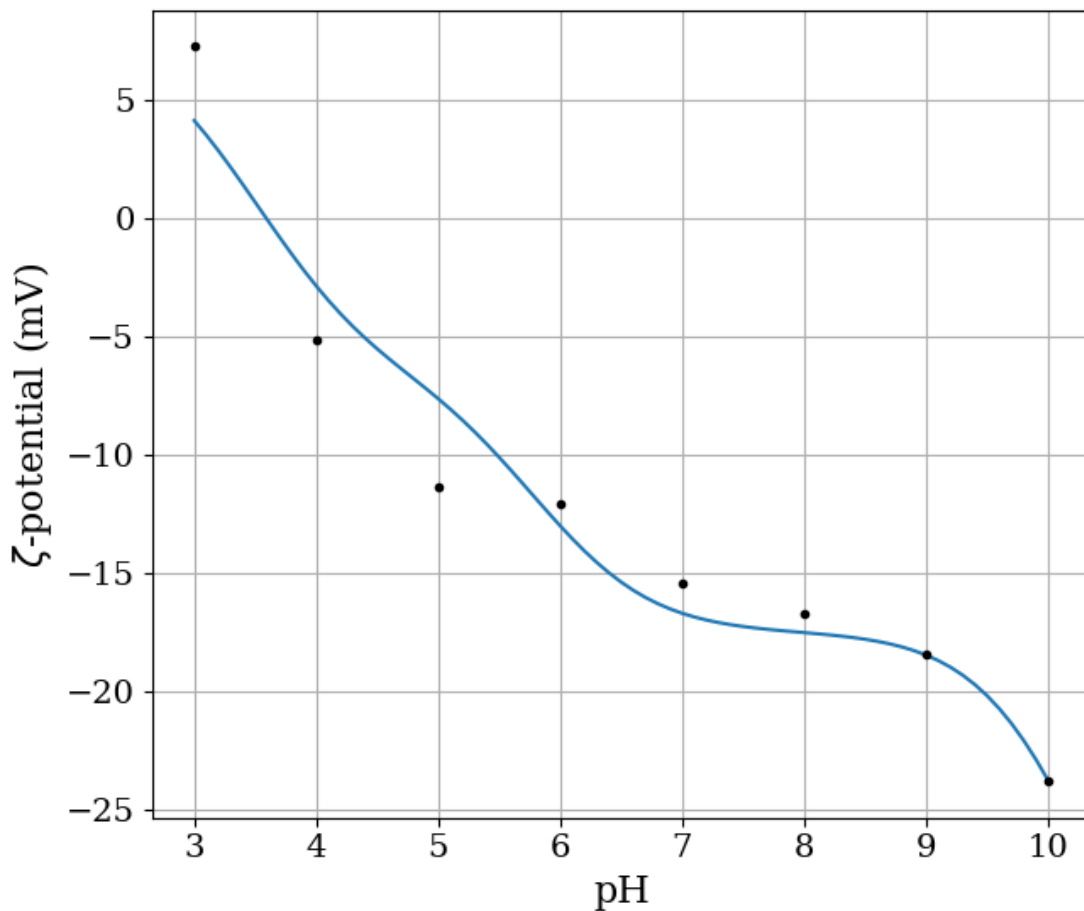
	$pK_{a,carboxyl}$	$pK_{a,phosphoryl}$	$pK_{a,hydroxyl}$	$pK_{a,amine}$
<b>10 mM</b>	3.51	5.6	10.39	10.39
<b>1 mM</b>	3.46	5.6	12.0	10.92

Source: The author, 2020.

With the new parameters, new curves for the zeta potential as a function of pH were obtained. In Figure 13 it is possible to see that for the ionic strength of 10 mM the curve for parameters reported in Table 6 the potential comes closer to experimental points for pH 6.0 and 8.0, but on the other hand get farther from the point of pH 7.0. For pH 5.0, although coming a little closer, the model still cannot capture the drop that happens in the zeta potential

experimental values. Overall, some improvement was achieved with the new estimation results, but the fitting is still not perfect.

Figure 13 – Zeta potential of *S. cerevisiae* as a function of pH for 10 mM with estimation of effectiveness coefficient and  $pK_a$  using a wider range



Legend: Modeled zeta potentials of *S. cerevisiae* are portrayed by the curve, whereas dots represent the experimental results of Narong and James (2006).

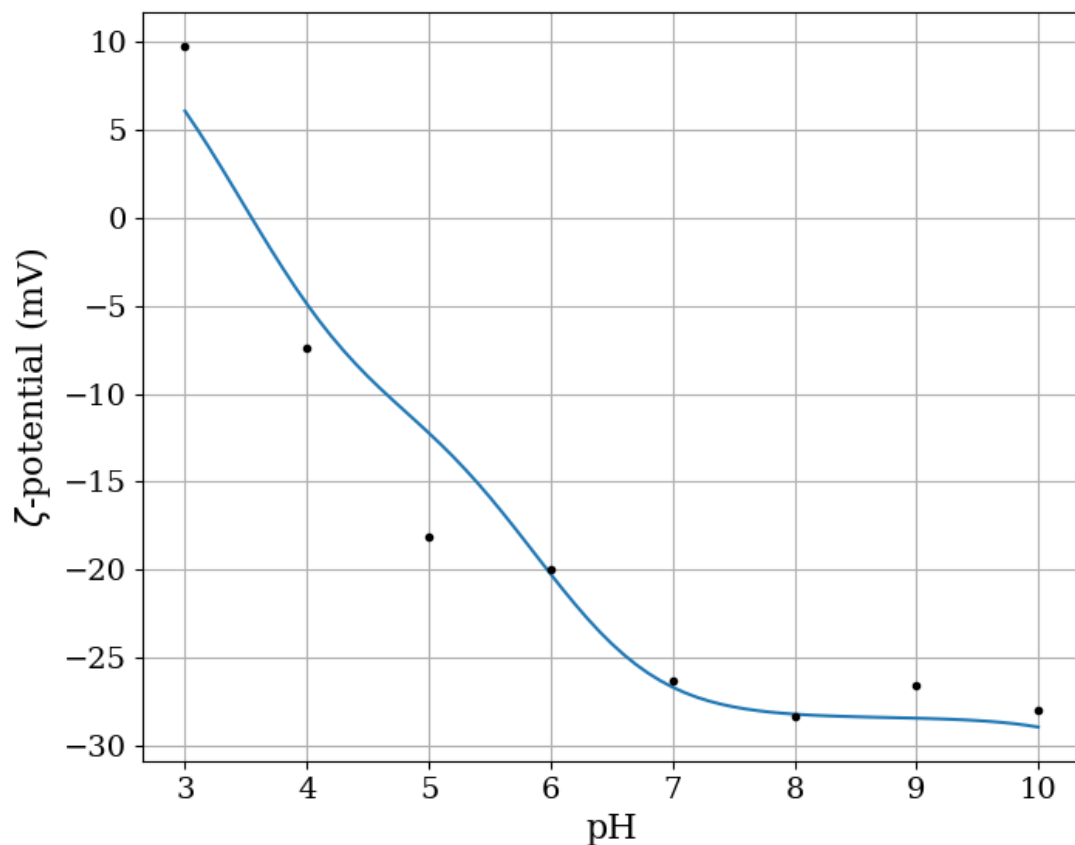
Source: The author, 2020.

Figure 14 presents a curve for the zeta potential as a function of pH calculated using the parameters on Table 6 for the ionic strength of 1mM. In it we can observe that from pH 5.0 to 8.0 the curve approached the experimental points, and from pH 8.0 to 10.0 the curve was able to reproduce the stagnation seen on experimental points. It appears that the reason why this curve is able to describe the stagnation of the experimental points is because of the high value of the  $pK_a$  of the hydroxyl group.

As said before, physically speaking a value high like 12.0 is not expected for the hydroxyl group, but mathematically speaking, what the method really does when it returns

this high value is that it disregards the dissociation of this group for the  $pK_a$  range of our calculations (pH 3.0 - 10.0). In fact, if we use the  $pK_a$  values of the first estimation and progressively diminish the amount of the hydroxyl group in our calculations, it is possible to see the curve approaching the experimental points and stabilizing near pH 8.0 (around -28 mV), just like for the high  $pK_a$  value obtained in the new estimation. A possible explanation for the experimental results of pH 8.0 - 10.0 is that the hydroxyl group may not be easily accessible at this ionic strength due to the conformation of the cell wall and hence cannot contribute to the cell surface charge (ABU-LAIL; CAMESANO, 2003). Other hypothesis could be that as the surface becomes more negative, the resulting surface potential increases the  $pK_a$  of the remaining acid groups (AMORY; ROUXHET, 1988).

Figure 14 – Zeta potential of *S. cerevisiae* as a function of pH for 1 mM with estimation of effectiveness coefficient and  $pK_a$  using a wider range



Legend: Modeled zeta potentials of *S. cerevisiae* are portrayed by the curve, whereas dots represent the experimental results of Narong and James (2006).

Source: The author, 2020.

### 3.2 Constant volume charge density model

In an attempt to better describe the surface charge on the cell wall, another model was tested to calculate the zeta potential of the *Saccharomyces cerevisiae* cell, the charge-regulated volume charge density model.

As mentioned before, the yeast cell surface is not smooth, in fact it is composed of many macromolecules that contain ionizable groups. As this layer can have significant thickness, these groups may be distributed anywhere inside the volume of the cell wall. Considering that ions can penetrate this volume of the cell wall, the charge-regulated volume charge density model proposes that the ionizable groups can be accounted for as being fixed charges distributed over the cell wall. With the fixed and mobile charges now being solved together in space, some assumptions were made in the resolution process. They were: the fixed charges are uniformly distributed over the cell wall; and the cell wall has an infinitely ion-penetrable layer (this assumption can be used when the thickness of the cell wall is much higher than the thickness of the double layer, usually the case for microbial cells).

Using this model, Barbosa, Lima and Tavares (2015) could successfully compute the zeta potential of the *B. brevis* bacteria without having to use an effectiveness coefficient to correct the number of functional groups. Knowing this, in this work we calculated the electrostatic potential for the *S. cerevisiae* using the charge-regulated volume density of charge model to check if we could achieve similar results.

Before computing the zeta potential, first the number of groups per volume was calculated. For this, the knowledge of the thickness of the cell wall was necessary. According to the study of Klis, de Koster and Brul (2014) the thickness of *S. cerevisiae* cell wall is 115 nm; hence dividing the numbers obtained in Table 3 (number of groups per surface area) by the thickness we can find the number of groups per volume. The corresponding results can be seen in Table 7.

Table 7 – Number of groups parameters for the charge-regulated volume charge density model

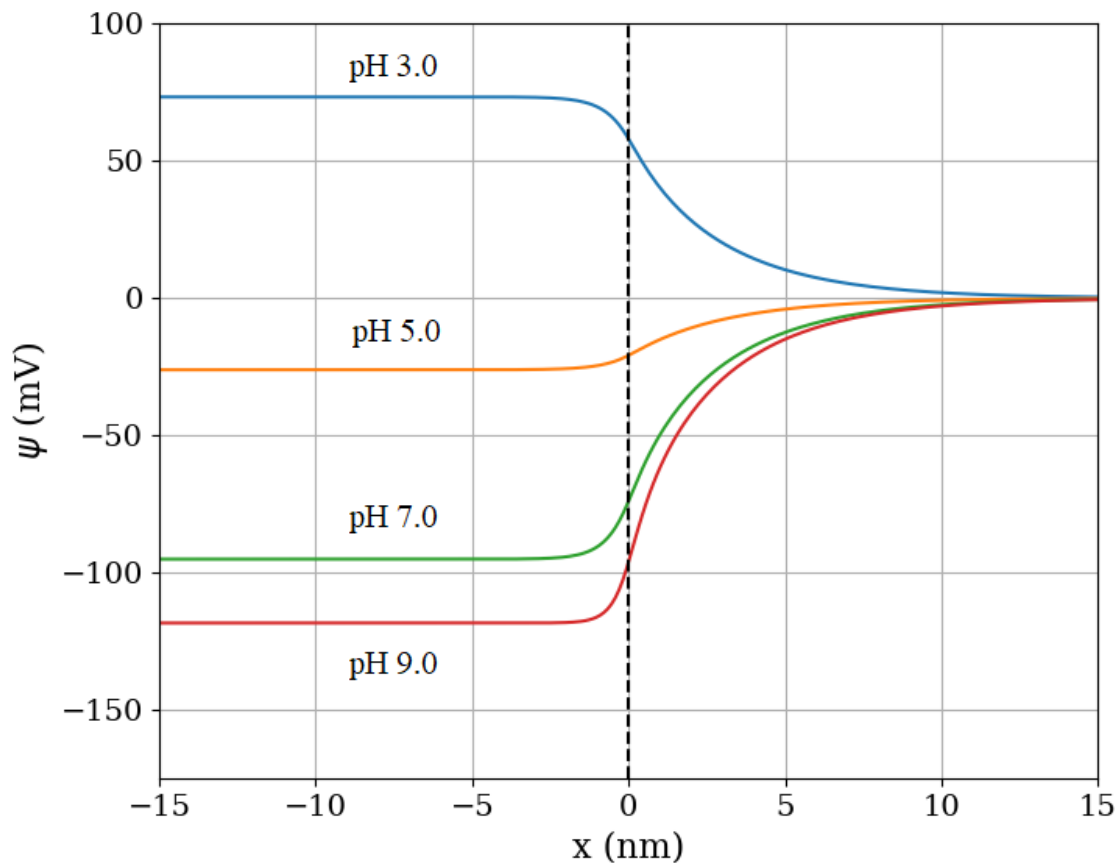
	<b>Carboxyl</b>	<b>Phosphoryl</b>	<b>Hydroxyl</b>	<b>Amine</b>
<b><i>N</i> (#/nm<sup>3</sup>)</b>	0.6478	0.5038	1.223	0.3599

Source: The author, 2019.

With the numbers in Table 7 the model was solved, and new electrostatic potential profiles were obtained for the two ionic strengths (1 mM and 10 mM). The first  $pK_a$  values used were the ones displayed in Table 2 (mean range values).

Results of the electrostatic potential as a function of distance for the new model can be seen in Figure 15 and Figure 16 for 10 mM and 1 mM (NaCl), respectively, for different pH values. The dashed black line in the graphs indicates the limit between the cell wall and the medium. We can notice for both figures that the potential varies a few nanometers into the cell wall (approximately 2 nm) until stabilizing and reaching the Donnan potential, that is the potential at the location where the fixed charges are fully compensated by the local diffuse charge density (POORTINGA et al., 2002).

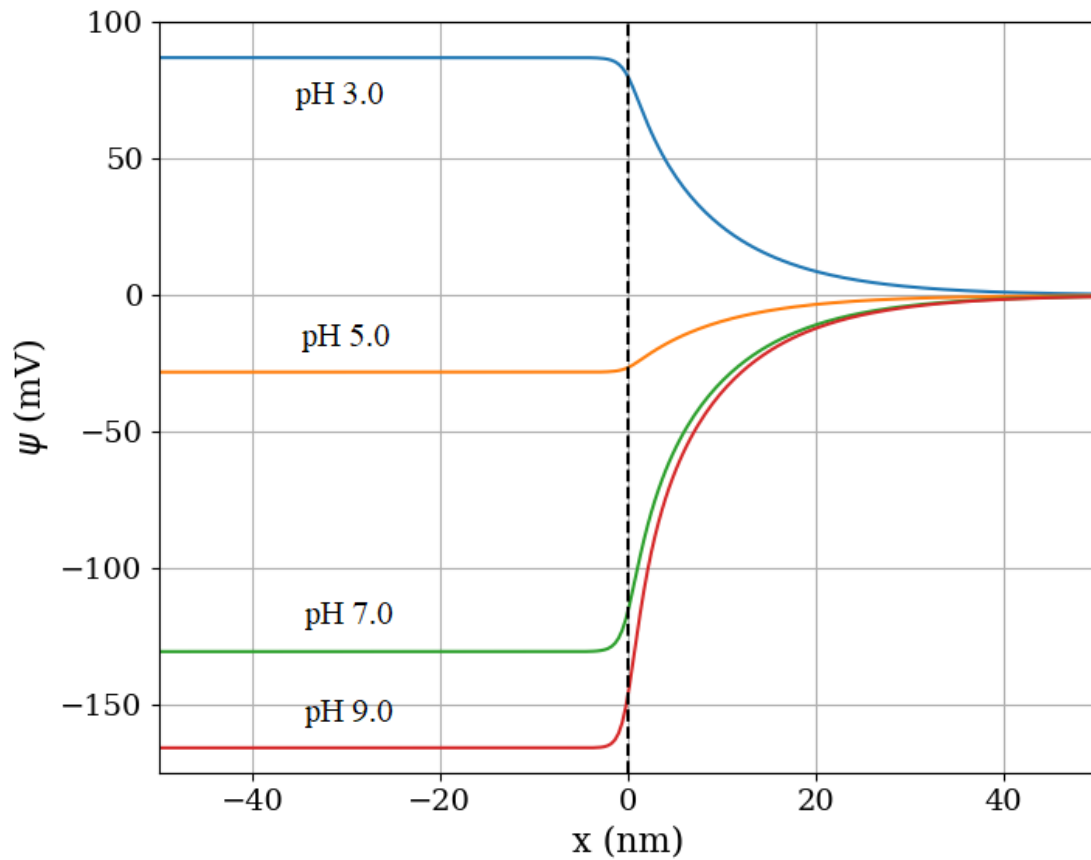
Figure 15 – Electrostatic potential profile computed by the charge-regulated volume charge density model for ionic strength of 10 mM (NaCl).



Legend: The dashed black line represents the limit between the cell wall and the medium.

Source: The author, 2020.

Figure 16 – Electrostatic potential profile computed by the charge-regulated volume charge density model for ionic strength of 1 mM (NaCl).



Legend: The dashed black line represents the limit between the cell wall and the medium.  
Source: The author, 2020.

Analyzing the values obtained in Figure 15 and Figure 16, it is possible to notice that the surface potential predicted by this model is lower (in magnitude) than for the charge regulation on the surface model: results for 10 mM and 1 mM at pH 7.0 are -73.8 mV and -116 mV, respectively, while the ones obtained in the previous model for the same system's conditions are around -146mV for both ionic strengths.

Another interesting observation we can make is that the potential calculated at the surface for this model is different for the different ionic strengths, something the other model could not predict. Comparing values at the Stern layer, the potential for 10 mM is -65.2mV and for 1 mM the value is -111mV, indicating that although calculated electrostatic potential values improved with this more sophisticated model, results in general are still significantly higher than experimental zeta potential values for the *S. cerevisiae* cell, not only for pH 7.0, but for all the range tested as well.

Unfortunately, this work could not achieve for *S. cerevisiae* the same success as Barbosa, Lima and Tavares (2015) for the *B. brevis* and in order to calculate a surface potential compatible with experimental results the use of the effectiveness coefficient was still necessary.

Comparing the cell walls of *S. cerevisiae* and *B. brevis* we notice that the *S. cerevisiae* yeast cell wall (115nm) is thicker than the one of the *B. brevis* bacteria (75nm). And maybe because of its larger thickness some groups deep inside the cell may not have a strong effect on the overall surface charge.

It is also worth pointing out one difference between this work and the work of Barbosa et al. (2015), the potentiometric titration experimental data (ZHANG et al., 2010) and zeta potential data (NARONG; JAMES, 2006) used here were taken from different sources, while in the study of Barbosa et al. (2015) these data were taken from the same research group (HONG; BROWN, 2006; 2008). Since different isolates with different surfaces can exist for the same strain or species (POORTINGA et al, 2002), we do not know what influence taking experimental results from different sources can have in our results.

Looking at the results for the first model, estimating all parameters together seemed more efficient, so we decided to estimate all parameters for this model as well, the effectiveness coefficient and the  $pK_a$  of the groups were estimated using the same conditions and same optimization method as before, the Sequential Least Squares Programming (SLSQP) algorithm implemented in the Python Scipy library. The ranges used as constrains for the  $pK_a$  values were the ranges found by Zhang et al. (2010) reported on Table 1.

Table 8 shows the results of the estimation for this model. Results for the  $pK_a$  parameters in general were not very different from the ones encountered in the estimation of the previous model, but the value for the effectiveness coefficient increased.

Table 8 – Estimation results for the volumetric charge density model

	$pK_{a,carboxyl}$	$pK_{a,phosphoryl}$	$pK_{a,hidroxyyl}$	$pK_{a,amine}$	$\lambda_{eff}$
<b>10 mM</b>	3.52	6.24	10.13	10.13	0.0301
<b>1 mM</b>	3.52	6.24	10.13	10.92	0.0053

Source: The author, 2020.

For 10 mM, the  $pK_a$  of the carboxyl and phosphoryl groups again landed at the lower boundary, but the  $pK_a$  of the hydroxyl and amine groups left the boundaries and their values matched at 10.13. The effectiveness coefficient value increased by a factor of 100, which

seems to be related to the fact we divided the number of groups by the cell wall thickness that is about 100 nm. Dividing the new coefficient value by the thickness of the cell wall (115nm), we find that the old and new values are quite comparable, around  $3 \times 10^{-4}$ .

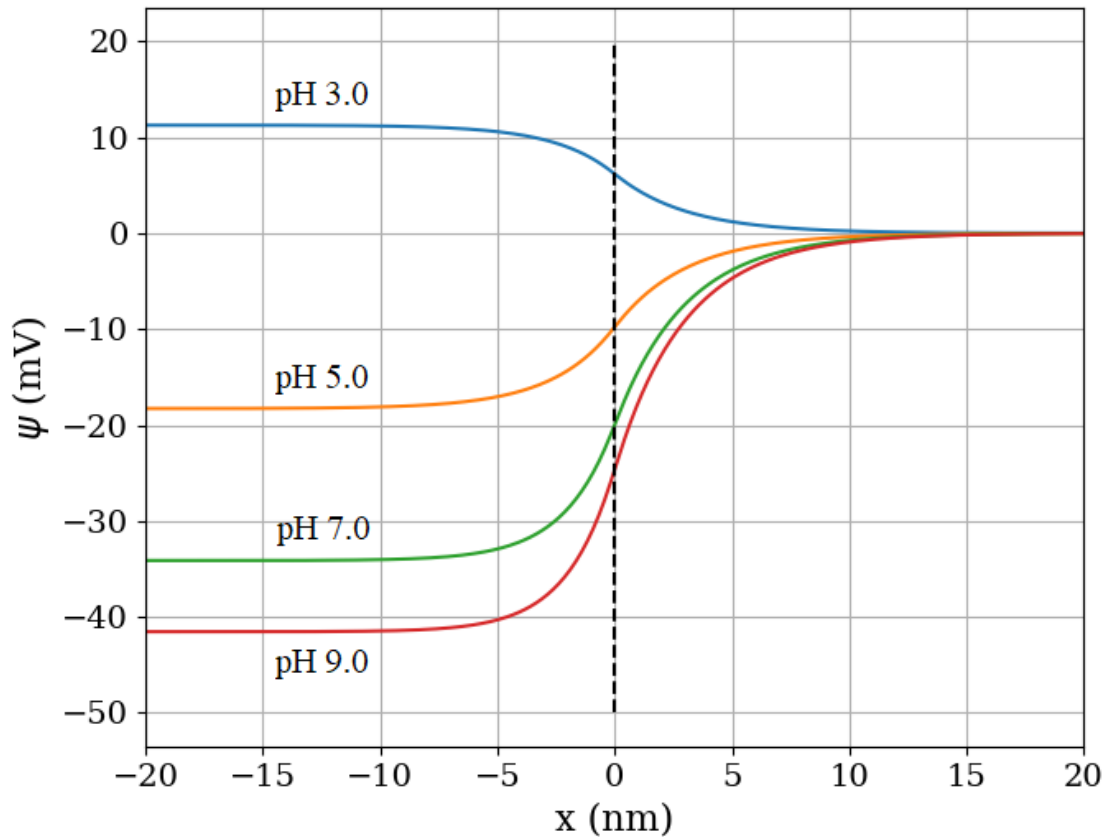
For 1 mM, all  $pK_a$  values remained the same, values for the carboxyl and phosphoryl groups landed at the lower boundaries and for the hydroxyl and amine groups landed at the upper boundaries. Having in view that the shape of experimental points for this ionic strength appears hard to describe using both models, this result does not come as a surprise since the optimization tries to push these values to the boundaries in order to obtain the best fit possible. The effectiveness coefficient value increased for this model, but not by a factor of 100 as observed for the ionic strength of 10 mM, and dividing the new value by the thickness of the cell wall a value three times smaller than the one encountered in the optimization for the first model is found.

Concerning the objective functions, the estimation for both ionic strengths showed gain in the minimization. For 10 mM, the value of the objective function went from 41 in the first model to 30 in this model, for 1 mM the gain was even larger, going from 164 in the previous model's estimation to 73 in this one.

With these values new calculations were performed. For each ionic strength, new graphs of the electrostatic potential as a function of distance were obtained and curves of the zeta potential as a function of pH were calculated using the charge-regulated volume density charge model with the effectiveness coefficient (Model 2) and the results were compared with the ones obtained using the charge regulation on the surface model (Model 1).

Figure 17 shows the electrostatic potential profile for the model with the estimated effectiveness coefficient for 10 mM. It is possible to observe that results at the surface and Stern layer are more consistent with experimental zeta potential values. One difference we can point in this curve compared to the previous one presented in Figure 15 is the distance from which the potential varies inside the cell wall, that now is of more than 5 nm, larger than the one predicted before (2 nm).

Figure 17 – Electrostatic potential profile computed by the charge-regulated volume charge density model with the effectiveness coefficient for ionic strength of 10 mM (NaCl).

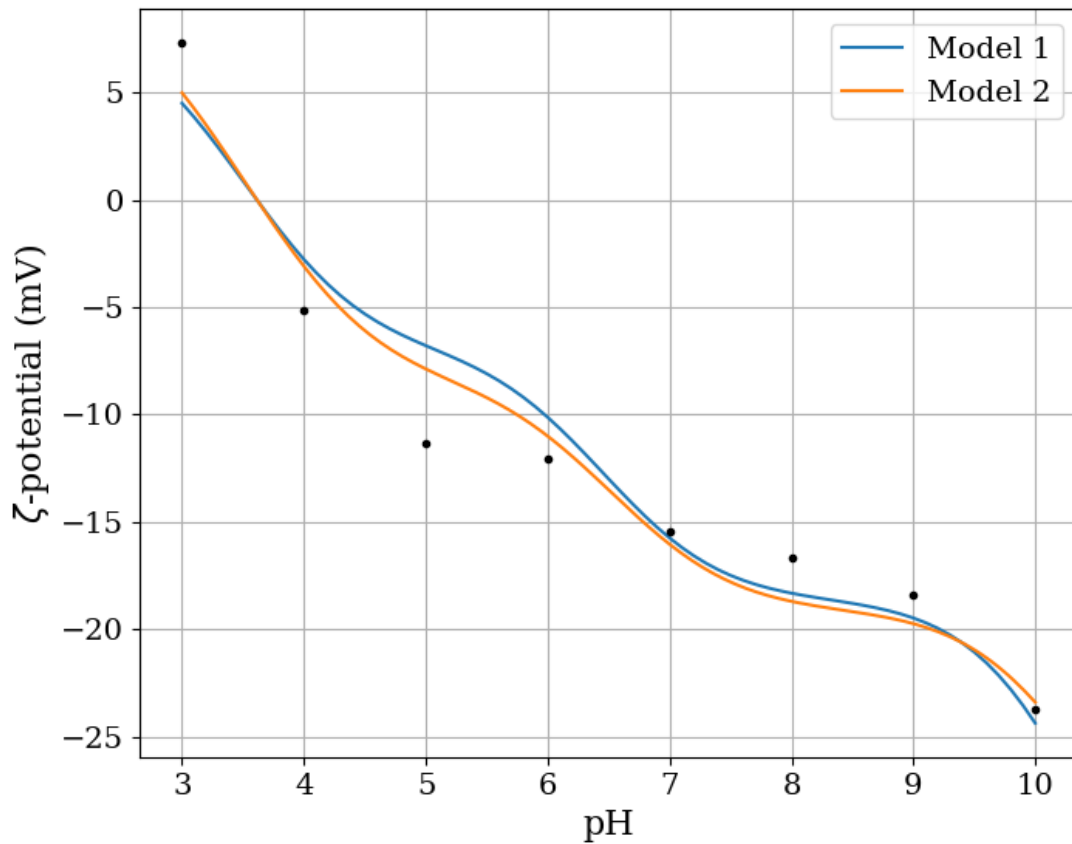


Legend: The dashed black line represents the limit between the cell wall and the medium.

Source: The author, 2020.

In Figure 18 we can see the curve for the zeta potential as a function of pH and how the results of the second model compare with the first one. Looking at the graph, neither curves can exactly capture the full shape of experimental points, but the second model seems to approach more the points on the first half of the curve, especially at pH 5.0 and 6.0. The first model comes closer to experimental points on the second half of the curve, but not by much. Overall, the second model provided a slight better fit for the experimental points than the first model. This was expected since the optimization for the second model had gain in the minimization of the objective function when compared to the one of the first model.

Figure 18 – Electrostatic potential of *S. cerevisiae* as a function of pH for ionic strength of 10 mM for the two models studied in this work.



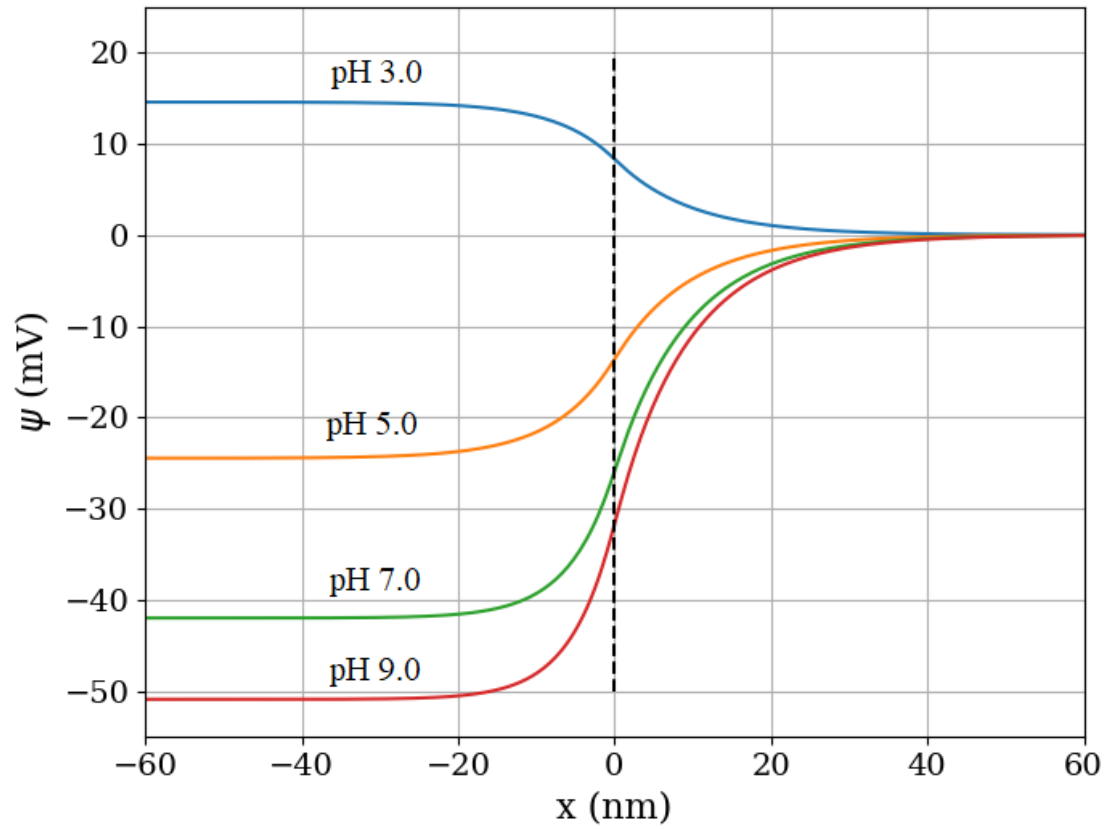
Legend: Modeled zeta potentials of *S. cerevisiae* are portrayed by the curve, whereas dots represent the experimental results of Narong and James (2006).

Source: The author, 2020.

The results for 1 mM are displayed in Figure 19 and Figure 20. Figure 19 shows the electrostatic potential as a function of distance and, just like for 10 mM, it is possible to notice that there was an increase in the distance from which the potential varies inside the cell wall. In Figure 16 this distance was around 2 nm and now in Figure 19 for the model with an effectiveness coefficient the distance is near 20 nm, an even higher increase than in the case for ionic strength of 10 mM.

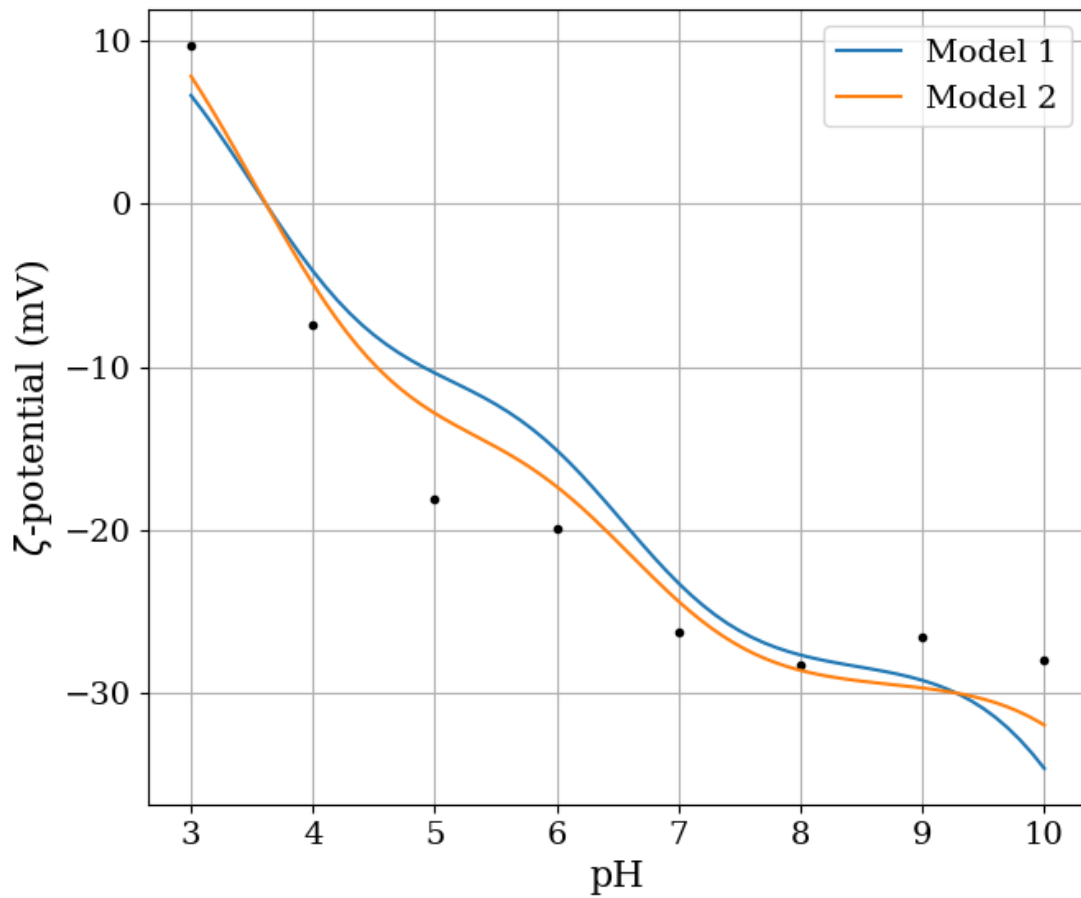
As for the results of zeta potential as a function of pH in Figure 20, the curve for the volumetric charge density model (Model 2) clearly shows a higher compatibility with experimental results than the first model. The curve for the second model comes closer to experimental values for practically all the pH range and for high pH values this curve shows a smoother decline in potential values that is more in agreement with the experimental values for that range.

Figure 19 – Electrostatic potential profile computed by the charge-regulated volume charge density model with the effectiveness coefficient for ionic strength of 10 mM (NaCl).



Legend: The dashed black line represents the limit between the cell wall and the medium.  
Source: The author, 2020.

Figure 20 – Electrostatic potential of *S. cerevisiae* as a function of pH for ionic strength of 1mM for the two models studied in this work.



Legend: Modeled zeta potentials of *S. cerevisiae* are portrayed by the curve, whereas dots represent the experimental results of Narong and James (2006).

Source: The author, 2020.

### 3.3 Parametric analysis results

Given that five parameters were estimated for the model, further analyses were performed to ensure that the best values were achieved on the estimation, such as. (i) an analysis of the sensitivity matrix to check for any parameter dependency and for more sensitive parameters; and (ii) a Monte Carlo test to analyze the relation of the  $pK_a$  parameters and the effectiveness coefficient.

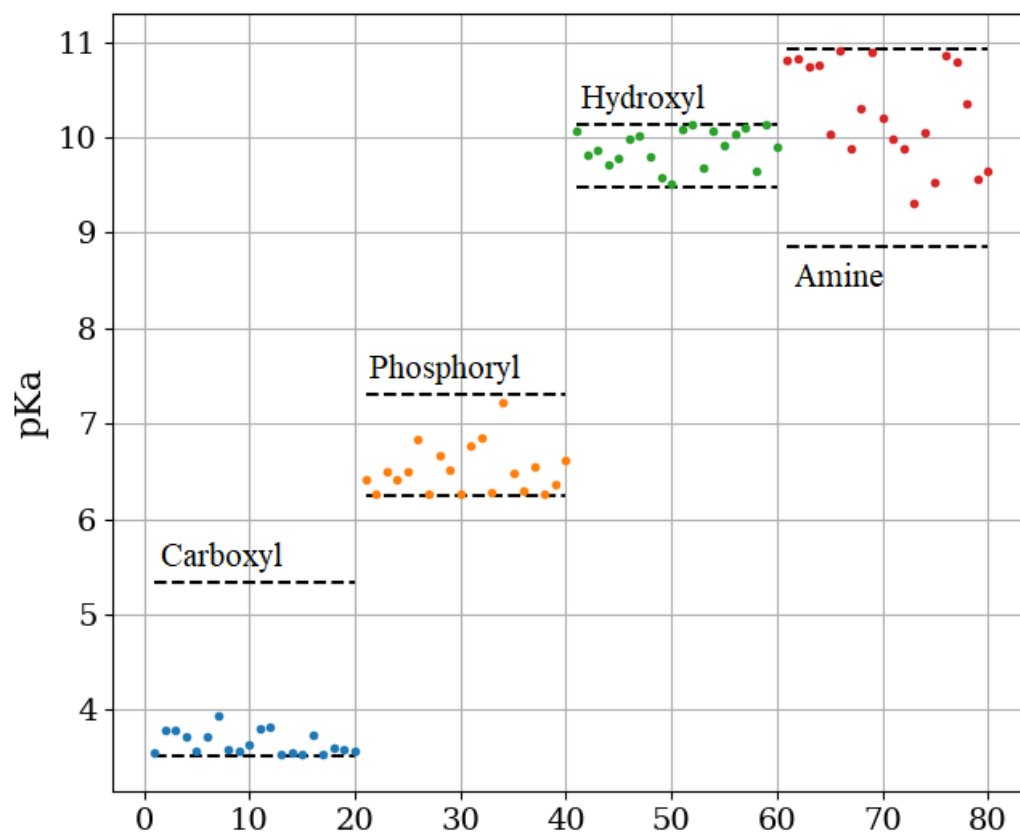
These parametric analyses were conducted only for the first model, the charge regulation on the surface.

### 3.3.1 Monte Carlo simulation

In this analysis a Monte Carlo simulation was performed for the  $pK_a$  parameters together with parameter estimation for the effectiveness coefficient. This strategy was used to obtain information on the relation of the  $pK_a$  parameters with the effectiveness coefficient. Random values used in the calculations were taken from the ranges reported by Zhang et al. (2010) presented on Table 2 and the effectiveness coefficient was estimated using the least-squares method and solve using the sequential linear squares programming algorithm implemented on Python.

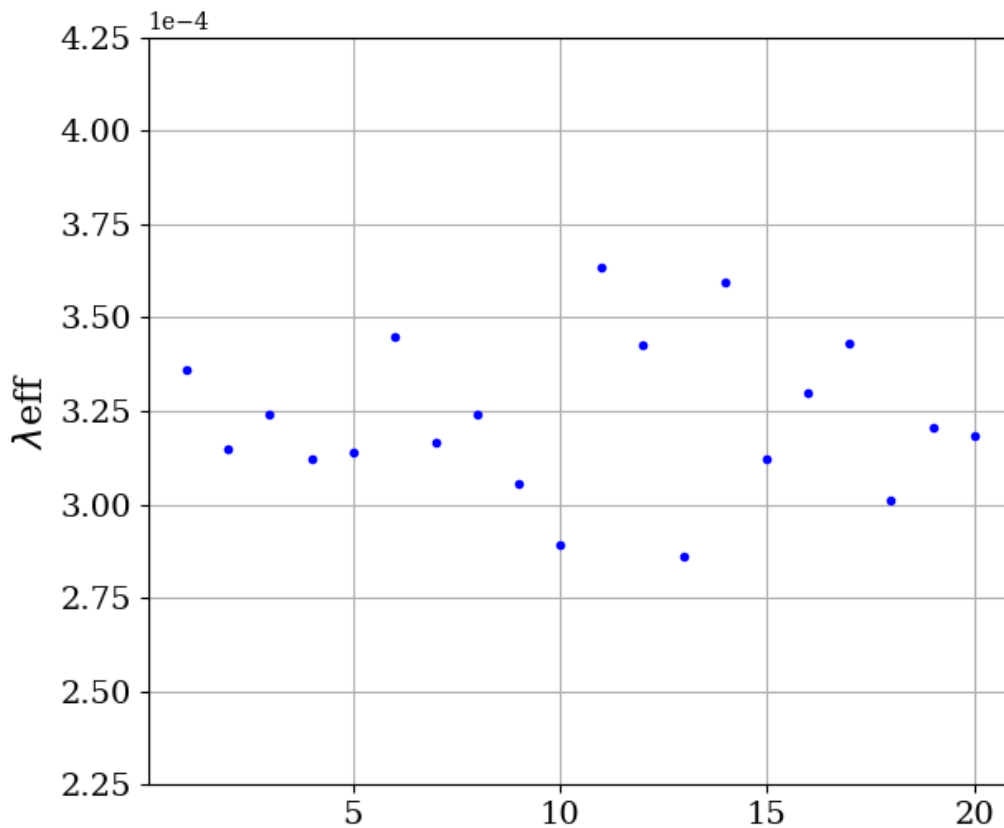
Because some sets of  $pK_a$  parameters and estimated effectiveness coefficient returned large values of the objective function, only parameters that provide a value of 72 or less for this function were considered, meaning that the model had a mean error of 3 mV for each point. In Figure 21 it is possible to see the random  $pK_a$  parameters values that that achieved the best results and in Figure 22 we can see that effectiveness coefficient values that were found in the estimations for the random  $pK_a$  parameters. In the figures, the x axis indicates the number of points and the y axis the value of the property analyzed.

Analyzing the  $pK_a$  parameters in Figure 21 we can observe where in the ranges reported in Table 2 lie the parameters that minimize the objective function. For the  $pK_a$  of the carboxyl and phosphoryl groups most values are located close to the lower boundaries; however, this happens more intensively for the carboxyl group. For the  $pK_a$  of the amine and hydroxyl groups, most values are located in the upper half of the range, being in general more dispersed than the values for the carboxyl and phosphoryl groups. For the effective coefficient in Figure 22 values vary mainly between  $3.0 \times 10^{-4}$  and  $3.5 \times 10^{-4}$ .

Figure 21 – pK<sub>a</sub> parameters of Monte Carlo simulation

Source: The author, 2020.

Figure 22 – Estimated effectiveness coefficient for the  $pK_a$  parameters



Source: The author, 2020.

### 3.3.2 Sensitivity matrix analysis

The sensitivity matrix, i. e., the matrix of the derivatives of the model in relation to the parameters, can provide information about how each parameter influences the model's results. By analyzing this matrix, it is possible to discover sensitive parameters and to determine if there is any dependency among the parameters.

In this analysis, the sensitivity matrix was calculated using the central finite difference numerical derivative for the zeta potential, and because there were different parameters with different orders of magnitude all values were normalized in order to perform a better analysis of the parameters.

The derivatives shown on Table 9 were calculated for ionic strength of 10 mM and pH values from 3.0 to 10.0 for the charge regulation model.

Table 9 – Normalized sensitivity matrix of the charge regulation on the surface model

$y(pH_i)$	$pK_{\text{carboxyl}}$	$pK_{\text{phosphoryl}}$	$pK_{\text{hidroxyl}}$	$pK_{\text{amine}}$	$\lambda_{\text{eff}}$
$y(3.0)$	3.474095	0.011762	0.000014	0.000004	0.901983
$y(4.0)$	-17.08109	-0.303270	-0.000360	-0.000106	0.870493
$y(5.0)$	-1.150951	-0.638129	-0.000791	-0.000233	0.947955
$y(6.0)$	-0.096952	-2.719776	-0.004767	-0.001402	0.916519
$y(7.0)$	-0.007187	-2.500931	-0.022125	-0.006508	0.869798
$y(8.0)$	-0.000701	-0.530697	-0.157993	-0.046477	0.919161
$y(9.0)$	-0.000066	-0.055876	-1.170382	-0.344294	0.886057
$y(10.0)$	-0.000005	-0.004422	-3.169017	-0.932236	0.716114

Source: The author, 2020.

As mentioned previously in section 1.6.2, by using the QR decomposition on the sensitivity matrix is possible to check the model for any dependency between parameters and also analyze which are the most sensitive parameters and least sensitive ones.

In Table 10 it is possible to see the diagonal elements of the pivoted matrix  $R$  and the rank result for both the default tolerance and for an established tolerance of  $10^{-7}$  (same tolerance of the numerical method). The QR decomposition with column pivoting and rank determination was performed using an algorithm implemented in the Scilab software.

Table 10 – Results of the QR decomposition of the sensitivity matrix

Diagonal element of pivoted matrix $R$				
$pK_{\text{carboxyl}}$	$pK_{\text{phosphoryl}}$	$pK_{\text{hidroxyl}}$	$\lambda_{\text{eff}}$	$pK_{\text{amine}}$
-17.4689	3.78265	-3.38144	1.51941	$2.3 \times 10^{-8}$
Rank (default tolerance)	5	Rank (tolerance = $10^{-7}$ )	4	

Source: The author, 2020.

Analyzing the results of the rank determination, to check if all of the parameters are uncorrelated, the rank calculated by the method for a default tolerance of Scilab algorithm was 5, the same number of columns/parameters. Nevertheless, when changing the tolerance to  $10^{-7}$  we see the rank number change to 4, suggesting that one parameter may be correlated: the  $pK_a$  of the amine group.

After checking the rank, the results of the diagonal elements of the pivoted matrix  $R$  were analyzed. The pivoting orders the columns of the matrix from most sensitive parameters (highest diagonal values) to least sensitive (lower diagonal values). Examining the results, it is possible to notice that the most sensitive parameter is the  $pK_a$  of the carboxyl group and second comes the  $pK_a$  of the phosphoryl group. Considering a rank equal to 5, the least sensitive parameter is the  $pK_a$  of the amine group, but when considering a rank of 4 and removing the  $pK_a$  of the amine group from the analysis, the parameter that shows the least sensitivity is the effectiveness coefficient.

Considering the questionable correlation of the amine's group  $pK_a$  parameter and the fact that correlated and least sensitive parameters are harder to be estimated, it was decided to carry out another parameter estimation, this time taking this group out of the estimation. Unfortunately, it was not possible to achieve any improvement in the fitting even taking the amine group out of the estimation.

## CONCLUSION

In this work, a study of the electrostatic behavior of the *S. cerevisiae* yeast cell wall was performed by using two theoretical models based on the Poisson-Boltzmann equation, the charge regulation model and the volumetric charge density model. The study showed that it was possible to reproduce values of experimental zeta potential over a range of pH, but this could only be achieved by using an effectiveness coefficient to correct the number of functional groups present on the cell wall. Without correcting the number of groups on the cell wall both models predicted values of zeta potential greater in magnitude than the values observed in experiments.

Another procedure that helped improve the fitting of both models was the parameter estimation of the  $pK_a$  of the functional groups. Since data for these parameters are usually reported as a range of values, a parameter estimation was it was conducted to find the best values to represent the yeast cell wall.

Both models yielded their best fitting for the experimental points when having all parameters estimated together. And, comparing the surface charge regulation model's results with the results of the volumetric density charge model, the latter seems to provide a better fit for the shape of experimental points, especially for the case of low concentration (1 mM), which was expected since the volumetric density charge model is a more adequate model for this system than the charge regulation model.

By performing parameter analysis, it was possible to obtain information on how the parameters are related to the charge regulation model. A Monte Carlo simulation for the  $pK_a$  groups revealed where in the  $pK_a$  ranges lie the values than can minimize the objective function. As result, parameters of the carboxyl and phosphoryl groups seem closer to the lower bounds of the ranges, while values for the hydroxyl and amine groups appears closer to the upper boundaries. Analyzing the sensitive matrix of the model using the QR decomposition we were able to identify the most and least sensitive parameters of the model. The most sensitive parameter identified was the  $pK_a$  of the carboxyl group, followed by the phosphoryl group. The least sensitive and probably dependent parameter was the  $pK_a$  of the amine group.

One difference from this work to the work of Hong and Brown (2008) and Barbosa et al. (2015) is that the results for the zeta potential and potentiometric titration experiments were taken from different sources while in the cited works they were taken from the same

source. This can have an impact in the study since the cell wall characteristics of different isolates may be different.

One suggestion for future works is the use of both zeta potential and potentiometric titration experiments for the same culture of *S. cerevisiae*, in order to improve the performance of the theoretical model.

Other good ideas for future works are the study of different effectiveness coefficients for the different groups and the study of the position of the slipping plane.

In this work, we had information about the functional groups that are present on the *S. cerevisiae* cell wall, but not on how they are arranged in the cell wall. It's possible that some types of groups may be more exposed on the surface while others may be located more on the inner part of the cell wall. A study on different effectiveness coefficients could help us understand more about how these groups are arranged and how they influence the surface charge.

About the slipping plane, it has been stated before that the position of the slipping plane in biological surfaces is uncertain. Further studies on the position of this plane can help model's achieve better results.

## REFERENCES

- ABU-LAIL, N. I.; CAMESANO, T. A. Role of Ionic Strength on the Relationship of Biopolymer Conformation, DLVO Contributions, and Steric Interactions to Bioadhesion of *Pseudomonas putida* KT2442. *Biomacromolecules*, v. 4, p. 1000-1012, 2003.
- AMORY, D. E.; ROUXHET, P. G. Surface properties of *Saccharomyces cerevisiae* and *Saccharomyces carlsbergensis*: chemical composition, electrostatic charge and hydrophobicity. *Biochimica et Biophysica Acta*, v. 938, p. 61-70, 1988.
- ARAÚJO, E. A. et al. Control of Microbial Adhesion as a Strategy for Food and Bioprocess Technology. *Food Bioprocess Technol*, v. 3, p. 321-332, 2010.
- ASRI, et al. Theoretical and Experimental Adhesion of Yeast Strains with High Chromium Removal Potential. *Environmental Engineering Science*, v. 34, n. 10, p. 693-702, 2017.
- BARBOSA, N. S. V.; LIMA, E.R.A.; TAVARES, F.W. The electrostatic behavior of the bacterial cell wall using a smoothing function to describe the charge-regulated volume charge density profile. *Colloids and Surface B: Biointerfaces*, v. 134, p. 447-452, 2015.
- BARKLEIT, A.; MOLL, H.; BERNHARD, G. Interaction of uranium(VI) with lipopolysaccharide. *Dalton Transactions*, 2008, p. 2879-2886.
- BATZEL, J. J.; BACHAR, M.; KAPPEL, F. *Mathematical Modeling and Validation in Physiology: Applications to the Cardiovascular and Respiratory Systems*. Berlin : Springer-Verlag, 2013.
- BOGGS, P. T.; TOLLE, J. W. Sequential quadratic programming. *Acta Numerica*, v.4, p. 1-51, 1995.
- BOWMAN, S.M.; FREE, S.J. The structure and synthesis of the fungal cell wall. *BioEssays*, v. 28, p. 799-808, 2006.
- CHO, K. H. et al. Experimental Designs in System Biology, Based on Parameter Sensitivity Analysis Using a Monte Carlo Method: A Case of Study for the TNF  $\alpha$ -Mediated NF- $\kappa$ B Signal Transduction Pathway. *Simulation*, v. 72, n. 12, p. 726-739, 2003.
- COSTANTINIDES, A.; MOSTOUFI, N. *Numerical Methods for Chemical Engineers with MATLAB Applications*. Upper Saddle River, NJ, United States: Prentice Hall PTR, 1999.
- DENGIS, P.B.; ROUXHET, P.G. Surface Properties of Top- and Bottom-Fermenting Yeast. *Yeast*, v. 13, p. 931-943, 1997.
- DEUFLHARD, P; ROBLITZ, S. *A Guide to Numerical Modelling in systems Biology*. Switzerland: Springer International Publishing, 2015.
- DI CAPRIO, F. et al. Mechanistic modeling of copper biosorption by wild type and engineered *Saccharomyces cerevisiae* biomasses. *Chem. Eng. J.*, v. 244, p. 561-568, 2014.

HERMANSSON, M. The DLVO theory in microbial adhesion. *Colloids and Surfaces B: Biointerfaces*, v. 14, p.105-119, 1999.

HONG, Y.; BROWN, D. G. Cell surface acid-base properties of *Escherichia coli* and *Bacillus brevis* and variation as a function of growth phase, nitrogen source and C:N ratio. *Colloids and Surfaces B: Biointerfaces*, v. 50, p. 112-119, 2006.

HONG, Y.; BROWN, D. G. Electrostatic Behavior of the Charge-Regulated Bacterial Cell Surface. *Langmuir*, v. 24, p. 5003-5009, 2008.

KLIS, F. M.; KOSTER, C. G.; BRUL, S. Cell Wall-Related Bionumbers and Bioestimates of *Saccharomyces cerevisiae* and *Candida albicans*. *Eukaryotic Cell*, v. 13, n. 1, p. 2-9, 2014.

LIMA, E. R. A. *Cálculo de Propriedades Físico-Químicas de sistemas coloidais via equação de Poisson-Boltzmann*. 2008. 144 f. Tese (Doutorado em Engenharia Química) Programa de Engenharia Química, COPPE/UFRJ, Rio de Janeiro, 2008.

LIMA, E. R. A.; TAVARES, F. W.; BISCAIA JR, E. C. Finite volume solution of the modified Poisson-Boltzmann equation for two colloidal particles. *Phys. Chem. Chem. Phys.*, v. 9 p. 3174-3180, 2007.

LIU, M. et al. Contribution of surface functional groups and interface interaction to biosorption of strontium ions by *Saccharomyces cerevisiae* under culture conditions. *RSC Adv.*, v. 7, p. 50880-50888, 2017.

MARSHALL, K.C.; BLAINEY, B.L. Role of Bacterial Adhesion in Biofilm Formation and Biocorrosion. In: Flemming HC., Geesey G.G. (Eds.) *Biofouling and Biocorrosion in Industrial Water Systems.*, Berlin, Springer, 1991.

NANOCOMPOSIX. *Zeta potential measures*. Disponível em: <<https://nanocomposix.com/pages/zeta-potential-measurements>>. Acesso em: 05 fev. 2020.

NAEEM, A.; WOERTZ, J. R.; FEIN, J. B. Experimental Measurement of Proton, Cd, Pb, Sr, and Zn Adsorption Onto the Fungal Species *Saccharomyces cerevisiae*. *Environ. Sci. Technol.* v. 40, p.5724-5729, 2006.

NARONG, P.; JAMES, A.E. Effect of pH on the  $\zeta$ -potential and turbidity of yeast suspensions. *Colloids and Surfaces A: Physicochem. Eng. Aspects*, v. 274, p. 130-137, 2006.

NELDER, J. A.; MEAD, R. A simplex method for function minimization. *Computer Journal*, v. 7, p. 308-313, 1965.

OHKI, S.; OHSHIMA, H. Electrochemistry of colloidal systems: Double layer phenomena. In: Caplan, S. R.; Miller, I. R.; Milazzo, G. (Eds) *Bioelectrochemistry: General Introduction*. Birkhauser Basel vol. 1, 1995.

PARVATHI, K.; NARESHKUMAR R.; NAGENDRAN, R. Manganese Biosorption Sites of *Saccharomyces cerevisiae*. *Environ. Technol.*, v. 28, p. 779-784, 2007.

POORTINGA, A. T. et al. Electric double layer interactions in bacterial adhesion to surfaces. *Surf. Sci. Rep.*, v. 47, p. 1-32, 2002.

RAO, K. H.; SUBRAMANIAN, S. Bioflotation and Bioflocculation of relevance to minerals Bioprocessing. In: Donati, E. R.; Sand, W. (Eds.), *Microbial Processing of Metal Sulfides*. Dordrecht: Springer, 2007.

RIJNAARTS, H. et al., DLVO and steric contributions to bacterial deposition in media of different ionic strengths. *Colloids and Surfaces B: Biointerfaces*, v. 14, p. 179-195, 1999.

ROGOWSKA, A. et al. The influence of different pH on the electrophoretic behaviour of *Saccharomyces cerevisiae* modified by calcium ions. *Scientific Reports*, v. 8 , p. 7261, 2018.

SALGIN, S.; SALGIN, U.; BAHADIR, S. Zeta Potentials and Isoelectric Points of Biomolecules: The Effects of Ion Types and Ionic Strengths. *Int. J. Electrochem. Sci.*, v. 7, p. 12404-12414, 2012.

SCHWEGMANN, H.; FEITZ, A. J.; FRIMMEL, F. H. Influence of the zeta potential on the sorption and toxicity of iron oxide nanoparticles on *S. cerevisiae* and *E. coli*. *Journal of Colloid and Interface Science*, v. 347, p. 43-48, 2010.

SHARP, J. M.; DICKINSON, R. B. Direct Evaluation of DLVO Theory for Predicting Long-Range Forces between a Yeast Cell and a Surface. *Langmuir*, v. 21, p. 8198-8203, 2005.

THONART, P; CUSTINNE, M.; PAQUOT, M. Zeta potential of yeast cells: application in cell immobilization. *Enzyme Microb. Technol.*, v. 4, p. 191-194, 1982.

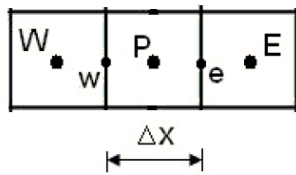
ZHANG, Y. et al. Study of the mechanisms of  $\text{Cu}^{2+}$  biosorption by ethanol/caustic-pretreated baker's yeast biomass. *J. Hazard. Mater.* v. 178, p. 1085-1093, 2010.

ZHAO, C. et al. Extracting local surface charges and charge regulation behavior from atomic force microscopy measurements at heterogeneous solid-electrolyte interfaces. *Nanoscale* v. 7, p. 16298-16311, 2015.

## APPENDIX A – Finite Volume Method

In developing the Finite Volume Method for the Poisson Boltzmann equation in one dimension, we start by dividing the domain into a number of volumes (n) and then we calculate the value of the desired property in the middle of the elementary volume, at the central point (P) using values from the volumes at east (W) and west (E).

Figure 23 – Elementary volume



Source: Adapted from LIMA; TAVARES; BISCAIA JR, 2007.

The following form will be used to develop the finite volume method for a generic unidimensional PB equation with uniform dielectric constant ( $\varepsilon$ ). Here  $S$ , the font term, is the right side of the PB equations, presented in equations (7) and (10) in the literature review chapter and  $y$  is the dimensionless electrostatic potential.

$$\frac{\partial}{\partial x} \left( \varepsilon \frac{\partial y}{\partial x} \right) = -S \quad (25)$$

To start the method, we integrate the equation in  $x$ , from the west boundary ( $w$ ) of the elementary volume to the east boundary ( $e$ ). After, we approximate the derivatives left using the central differences approximation.

$$\int_w^e \frac{\partial}{\partial x} \left( \varepsilon \frac{\partial y}{\partial x} \right) dx = - \int_w^e S dx \quad (26)$$

$$\Gamma_e \frac{y_E - y_P}{\Delta x} - \Gamma_w \frac{y_P - y_W}{\Delta x} = -S \Delta x \quad (27)$$

Multiplying both sides by  $\Delta x$  and rearranging the terms for  $\varphi$ :

$$\Gamma_e y_E - (\Gamma_e + \Gamma_w) y_P + \Gamma_w y_W = -S \Delta x^2 \quad (28)$$

Because the font term  $S$  is not a linear function, it is necessary to linearize it in order to achieve a linear system of algebraic equations. The linearization of the font term is obtained by using the Taylor series approximation truncated on the first order term.

$$\Gamma_e y_E - (\Gamma_e + \Gamma_w) y_P + \Gamma_w y_W = -y_P S_p \Delta x^2 - S_c \Delta x^2 \quad (29)$$

Rearranging again for  $y$  we get the final form of the equation:

$$\Gamma_e y_E - (\Gamma_e + \Gamma_w - S_p \Delta x^2) y_P + \Gamma_w y_W = -S_c \Delta x^2 \quad (30)$$

Each elementary volume generates an equation like equation (30), so as a result we are left with a tridiagonal system of  $n$  linear equations to solve. In which  $A$  is a tridiagonal matrix,  $b$  is the vector of independent terms and  $y$  is the term we want to solve for.

$$A \cdot y = b \quad (31)$$

The resulting terms for the diagonals of matrix  $A$  ( $d$  main diagonal,  $l$  lower diagonal and  $u$  upper diagonal) and  $b$  (independent vector) are:

$$l = \Gamma_w \quad (32)$$

$$u = \Gamma_e \quad (33)$$

$$d = -(\Gamma_e + \Gamma_w - S_p \Delta x^2) \quad (34)$$

$$b = -S_c \Delta x^2 \quad (35)$$

The terms for the upper and lower diagonal ( $\Gamma_e$  and  $\Gamma_w$ ) for both models have a value of 1. The terms obtained in the linearization of the font term ( $S_p$  and  $S_c$ ) for each model can be seen in Table 11, they were calculated for the dimensionless form of the PB equation.

Table 11 – Linearized font terms for the dimensionless PB equations

$S_p$	$-dS(y^*)$
$S_c$	$S(y^*) - y^* dS(y^*)$

With  $dS$  being the derivative of the font term  $S$ , and  $y^*$  being the value of  $y$  for the previous iteration.

The dimensionless form of the PB equation and the PB equation with fixed charges are:

$$S = -\frac{\sum_i z_i c_{i,0} \exp(-z_i y)}{\sum_i z_i c_{i,0}} \quad (36)$$

$$S = -\frac{\sum_i z_i c_{i,0} \exp(-z_i y)}{\sum_i z_i c_{i,0}} - \frac{\rho_f}{\sum_i z_i c_{i,0}} \quad (37)$$

With  $\rho_f$  being the yeast surface charge function presented in equation (19).

To solve the Poisson-Boltzmann equation in the dimensionless form, the variables used on the method also need to be dimensionless. The dimensionless potential ( $y$ ) and the Debye length ( $\kappa$ ), factor used to transform the spatial variables into dimensionless variables, are:

$$y = \psi e / k_B T \quad (38)$$

$$\kappa = \frac{N_A e^2 \sum_i z_i^2 c_{i,0}}{\varepsilon_0 \varepsilon_w k_B T} \quad (39)$$

For the unidimensional case two boundary conditions are necessary, one for the first volume and one for the last. The boundary condition type used in the resolution of both models described the value of the derivative of the property at the boundary.

$$\Gamma_e \frac{y_E - y_P}{\Delta x} - \left( \frac{dy}{dx} \Big|_{x \rightarrow initial} \right) = -S \Delta x \quad (40)$$

$$\left(\frac{dy}{dx}\right)_{x \rightarrow final} - \Gamma_w \frac{y_P - y_W}{\Delta x} = -S\Delta x \quad (41)$$

Inserting the derivatives at the boundary for each model and rearranging the equations in terms of  $y$ , we find the values of the main, upper and lower diagonals of matrix  $A$  and the independent vector  $b$ , for the first and last volumes of the method.

For the charge regulation model, the derivative at the boundary of the first volume is the yeast surface charge function described in equation (19) of chapter 2. This function is non-linear and to enter the method it also must be linearized, for this the expansion using the Taylor series truncated on the first-order term was again used. In this linearized equation, the term part multiplies  $y$  enters as a contribution to the main diagonal ( $d$ ) term and the other part of the term enters as contribution to the independent term ( $b$ ).

For the last volume in this model the derivative is equal to zero, making the deduction of the term for this volume quite simple.

For the volumetric charge density model both derivatives are zero, so for this model the deduction both terms are rather simple.